(12) INTERNATIONAL APPLICATION PUBLISHED UNDER THE PATENT COOPERATION TREATY (PCT)

(19) World Intellectual Property Organization
International Bureau

(43) International Publication Date
17 June 2010 (17.06.2010)

PCT

(10) International Publication Number
WO 2010/068282 A2

(51) International Patent Classification:
H01L 31/042 (2006.01)

(21) International Application Number:
PCT/US2009/006508

(22) International Filing Date:
10 December 2009 (10.12.2009)

(25) Filing Language: English

(26) Publication Language: English

(30) Priority Data:
61/201,440 10 December 2008 (10.12.2008) US

(71) Applicant *(for all designated States except US)*: **THE REGENTS OF THE UNIVERSITY OF CALIFORNIA** [US/US]; University Of California Office Of The President, 1111 Franklin Street 5th Floor, Oakland, CA 94607 (US).

(72) Inventors; and

(75) Inventors/Applicants *(for US only)*: **ZHANG, Jin, Zhong** [US/US]; Department Of Chemistry And Biochemistry, University Of California, Santa Cruz, CA 95064 (US). **WOLCOTT, Abraham** [US/US]; Department Of Chemistry And Biochemistry, University Of California, Santa Cruz, CA 95064 (US). **HENSEL, Jennifer** [US/US]; Department Of Chemistry And Biochemistry, University Of California, Santa Cruz, CA 95064 (US). **LOPEZ-LUKE, Tzarara** [US/US]; Department Of Chemistry And Biochemistry, University Of California, Santa Cruz, CA 95064 (US). **LI, Yat** [—/US]; Department Of Chemistry And Biochemistry, University Of California, Santa Cruz, CA 95064 (US).

(74) Agents: **KASER, Matthew** et al.; Bell & Associates, 58 West Portal Avenue, #121, San Francisco, CA 94127 (US).

(81) Designated States *(unless otherwise indicated, for every kind of national protection available)*: AE, AG, AL, AM, AO, AT, AU, AZ, BA, BB, BG, BH, BR, BW, BY, BZ, CA, CH, CL, CN, CO, CR, CU, CZ, DE, DK, DM, DO, DZ, EC, EE, EG, ES, FI, GB, GD, GE, GH, GM, GT, HN, HR, HU, ID, IL, IN, IS, JP, KE, KG, KM, KN, KP, KR, KZ, LA, LC, LK, LR, LS, LT, LU, LY, MA, MD, ME, MG, MK, MN, MW, MX, MY, MZ, NA, NG, NI, NO, NZ, OM, PE, PG, PH, PL, PT, RO, RS, RU, SC, SD, SE, SG, SK, SL, SM, ST, SV, SY, TJ, TM, TN, TR, TT, TZ, UA, UG, US, UZ, VC, VN, ZA, ZM, ZW.

(84) Designated States *(unless otherwise indicated, for every kind of regional protection available)*: ARIPO (BW, GH, GM, KE, LS, MW, MZ, NA, SD, SL, SZ, TZ, UG, ZM, ZW), Eurasian (AM, AZ, BY, KG, KZ, MD, RU, TJ, TM), European (AT, BE, BG, CH, CY, CZ, DE, DK, EE, ES, FI, FR, GB, GR, HR, HU, IE, IS, IT, LT, LU, LV, MC, MK, MT, NL, NO, PL, PT, RO, SE, SI, SK, SM, TR), OAPI (BF, BJ, CF, CG, CI, CM, GA, GN, GQ, GW, ML, MR, NE, SN, TD, TG).

[Continued on next page]

(54) Title: COMPOSITIONS AND METHODS FOR SYNTHESIS OF HYDROGEN FUEL

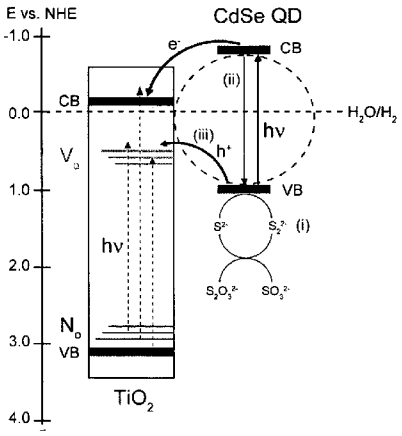

Figure 15

(57) Abstract: The invention provides new methods and compositions for synthesizing hydrogen fuel using simple and inexpensive materials.

WO 2010/068282 A2

Published:

— *without international search report and to be republished upon receipt of that report (Rule 48.2(g))*

COMPOSITIONS AND METHODS FOR SYNTHESIS OF HYDROGEN FUEL

This invention was made partly using funds from US Department of Energy (USDOE) research grant number DE-FG02-05ER46232-A002, and the United States National Science Foundation, Major Research Instrumentation (MRI) Program grant number CHE-0521569. The US Federal Government has certain rights to this invention.

Field of the Invention

The invention is drawn to novel compositions and methods for generating an electric current. The invention also provides novel compositions and methods for generating hydrogen as a fuel.

Background of the Invention

In recent years there is an increasing interest to find sustainable alternative energy (SAE) sources due to the heightening cost of fossil fuels and the detrimental effects of global climate change. Photovoltaic (PV) cells have received significant attention due to the limitless influx of photons from the sun. Recent market energy analysis is predicting energy parity between conventional energy production and PV costs in cents per kilowatt hour (cents/kWh) in only 5-8 years (LoPiccolo, P. *Solid State Technology* 2007, *50*, 2). Efficiency of silicon solar cells have attained a solar conversion efficiency of 20%, however the manufacturing process is very expensive and involves the use of toxic chemicals inherit in the semiconductor industry.

To date, there have been reports of two types of solar cells based on nanostructured semiconductor materials: the Grätzel solar cell, based on dye sensitized nanoporous semiconductor thin films and the quantum dot solar cell, based on composite films of semiconductor nanoparticles (CdSe) and conjugated polymers studied by Greenham et al. (see, for example, O'Regan, B.; Gratzel, M. *Nature* 1991, *353*, 737; Greenham, N. C.; Peng, X. G.; Alivisatos, A. P. *Phys. Rev. B* 1996, *54*, 17628). Grätzel's initial report in 1991 presented a nanocrystalline dye-sensitized solar cell converting light to electrical energy with an efficiency of 7% (O'Regan et al. *supra*). The dye-sensitized solar cell

(DSSC) consists of TiO_2 nanoparticles acting as a highly porous wide-bandgap semiconductor electron acceptor layer. In the DSSC visible light absorbing dye molecules adsorbed onto the TiO_2 surface act as the sensitizer to harvest more of the solar flux. Under irradiation, the photoexcited dye molecules inject electrons to the TiO_2 layer that are transported through the porous TiO_2 layer and collected by a conductive fluorine doped SnO_2 layer on the glass surface. The oxidized dye is regenerated by a liquid electrolyte, with the highest reported efficiency of about 10%. Greenham et al. (*supra*) investigated the processes of charge separation and transport in the interface between a conjugated polymer and semiconductor nanocrystal as a hybrid organic-inorganic system. A quantum efficiency of up 12% has been reported with a high concentration of nanocrystals, where both nanocrystals and polymers provide continous pathways to the electrodes (Greenham et al. *supra*). The absorption, charge separation and transport properties of the composities were found to be a function of the size, material and the surface ligands of the nanocrystals utilized.

TiO_2 and ZnO nanoparticles represent good examples of nanocrystalline materials used for potentially low cost PV devices for energy conversion, as an alternative to silicon solar cell technology and for photocatalysis (Belver, C.; Bellod, R.; Fuerte, A.; Fernandez-Garcia, M. *Applied Catalysis B-Environmental* **2006**, *65*, 301; Gregg, B. A. *J. Phys. Chem. B* **2003**, *107*, 4688; Hagfeldt, A.; Gratzel, M. *Accounts of Chemical Research* **2000**, *33*, 269; Kamat, P. V. *J. Phys. Chem. C* **2007**, *111*, 2834; Lokhande, C. D.; Park, B. O.; Park, H. S.; Jung, K. D.; Joo, O. S. *Ultramicroscopy* **2005**, *105*, 267; Smestad, G. P.; Spiekermann, S.; Kowalik, J.; Grant, C. D.; Schwartzberg, A. M.; Zhang, J.; Tolbert, L. M.; Moons, E. *Solar Energy Materials Solar Cells* **2003**, *76*, 85; Khaselev, O.; Turner, J. A. *Science* **1998**, *280*, 425; and Parsons, C. A.; Peterson, M. W.; Thacker, B. R.; Turner, J. R.; Nozik, A. J. *J. Phys. Chem.* **1990** *94*, 3381). Titanium dioxide (TiO_2), or titania, exists in three crystalline phases: anatase, rutile and brookite. Anatase and rutile have found uses mainly in PV cells, photoelectrochemical cells (PEC), and photocatalysis applications (Colon, G.; Maicu, M.; Hidalgo, M. C.; Navio, J. A. *Applied Catalysis B-Environmental* **2006**, *67*, 41; Kim, Y. G.; Walker, J.; Samuelson, L. A.; Kumar, J. *Nano Letters* **2003**, *3*, 523; Toyoda, T.; Tsuboya, I.; Shen, Q. *Materials Science & Engineering C-Biomimetic*

Supramolecular Systems **2005**, *25*, 853; and Wang, J. W.; Zhu, W.; Zhang, Y. Q.; Liu, S. X. *J. Phys. Chem. C* **2007**, *111*, 1010). On the contrary, the brookite phase has not received similar attention, perhaps because it is the most difficult to prepare in the form of a thin film (Djaoued, Y.; Bruning, R.; Bersani, D.; Lottici, P. P.; Badilescu, S. *Mater.Letters* **2004**, *58*, 2618). Titania has a wide band gap (3.2 eV) and absorbs only 5% of the solar spectrum, resulting in poor conversion efficiency in solar cell applications. Non metal-doped TiO_2 nanoparticles and nanotubes have been shown to produce electronic states in the TiO_2 bandgap, thereby extending photoresponse to the visible region and improving photoactivity (Huang, D. G.; Liao, S. J.; Liu, J. M.; Dang, Z.; Petrik, L. *J. Photochem. Photobio. A-Chem.* **2006**, *184*, 282; Huang, L. H.; Sun, Z. X.; Liu, Y. L. *J. Ceramic Soc. Jap.* **2007**, *115*, 28; Nishijima, K.; Naitoh, H.; Tsubota, T.; Ohno, T. *J. Ceramic Soc. Jap.* **2007**, *115*, 310). Recent studies of TiO_2:N and ZnO:N have found success in narrowing the bandgap and increasing light harvesting efficiency with nitrogen doping, and research has been focusing on the resulting photoelectro-chemical properties and photocatalytic activity for SAE production. Several different synthesis protocols have been developed to produce TiO_2:N. The usual doping process involves using ammonia as a nitrogen source by sol-gel, thermal, or hydrothermal chemical methods (Moribe, S.; Ikoma, T.; Akiyama, K.; Zhang, Q. W.; Saito, F.; Tero-Kubota, S. *Chem. Phys. Lett.* **2007**, *436*, 373; Sathish, M.; Viswanathan, B.; Viswanath, R. P.; Gopinath, C. S. *Chem. Mater.* **2005**, *17*, 6349; Beranek, R.; Kisch, H. *Electrochem. Commun.* **2007**, *9*, 761; Chen, H. Y.; Nambu, A.; Wen, W.; Graciani, J.; Zhong, Z.; Hanson, J. C.; Fujita, E.; Rodriguez, J. A. *J. Phys. Chem. C* **2007**, *111*, 1366; and Yin, S.; Ihara, K.; Aita, Y.; Komatsu, M.; Sato, T. *J.Photochem. Photobio.A-Chem.* **2006**, *179*, 105).

An alternative method to obtain TiO_2:N involves using hexamethylenetetramine (HMT) by chemical and mechanochemical processes. The resulting effect on crystalline phase composition showed increased photocatalytic activity and photovoltaic properties, with specific morphologies produced (Wu, J. M.; Qi, B. *J. Phys. Chem. C* 2007, *111*, 666; Yin, S.; Komatsu, M.; Zhang, Q. W.; Saito, F.; Sato, T. *J. Mater. Science* **2007**, *42*, 2399). Nitrogen doping within TiO_2 can be interstitial or substitutional, with the latter being more effective, resulting in mixing of N 2p states with O 2p states, and contributing to the

bandgap narrowing. Different techniques have been used to study N doped TiO_2 crystallographically, including XPS, EPR, Raman spectroscopy and XRD and absorption spectroscopy (see Chen and Burda *J. Phys. Chem. B* **2004**, *108*, 15446; Reyes-Garcia et al. *J. Phys. Chem. C* **2007**, *111*, 2738; and Wan et al. *Appl. Surf. Sci.* **2007**, *253*, 4764). Theoretical studies have supported the visible absorption and the resulting yellowish color of TiO_2:N thin films and powders (see, for example, Asahi, R.; Morikawa, T.; Ohwaki, T.; Aoki, K.; Taga, Y. *Science* **2001**, *293*, 269; Di Valentin, C.; Pacchioni, G.; Selloni, A.; Livraghi, S.; Giamello, E. *J. Phys. Chem. B* **2005**, *109*, 11414; Chen and Burda *supra*; Reyes-Garcia et al. *supra*; Wan et al. *supra*; Livraghi, S.; Paganini, M. C.; Giamello, E.; Selloni, A.; Di Valentin, C.; Pacchioni, G. *J. Am. Chem. Soc.* **2006**, *128*, 15666; and Burda, C.; Lou, Y. B.; Chen, X. B.; Samia, A. C. S.; Stout, J.; Gole, J. L. *Nano Letters* **2003**, *3*, 1049).

Alternative techniques to increase the photoresponse besides doping include the utilization of tunable narrow bandgap semiconductor nanoparticles or quantum dots (QDs) such as CdS, CdSe, and CdTe to sensitize wide bandgap semiconductors such as the metal oxides, e.g. TiO_2 and ZnO (Leschkies, K. S.; Divakar, R.; Basu, J.; Enache-Pommer, E.; Boercker, J. E.; Carter, C. B.; Kortshagen, U. R.; Norris, D. J.; Aydil, E. S. *Nano Letters* **2007**, *7*, 1793; Levy-Clement, C.; Tena-Zaera, R.; Ryan, M. A.; Katty, A.; Hodes, G. *Adv. Mater.* **2005**, *17*, 1512; Robel, I.; Kuno, M.; Kamat, P. V. *J. Am. Chem. Soc.* **2007**, *129*, 4136; and Somasundaram, S.; Chenthamarakshan, C. R.; de Tacconi, N. R.; Ming, Y.; Rajeshwar, K. *Chem. Mater.* **2004**, *16*, 3846). QDs with their large extinction coefficient strongly absorb visible light and inject electrons into the conduction band of metal oxides, and thereby contribute to increased solar energy conversion. Attachment of CdSe QDs to nanocrystalline TiO_2 has been shown to be successful with an immersion method using a bimolecular linker (Robel, I.; Subramanian, V.; Kuno, M.; Kamat, P. V. *J. Am. Chem. Soc.* **2006**, *128*, 2385). Sonochemical, photodeposition, and chemical bath deposition of CdSe on TiO_2 nanoparticles and nanotubes has also been studied for photocatalysis applications (Liu, H. Y.; Gao, L. *J. Am. Ceramic Soc.* **2005**, *88*, 1020; Nguyen, V. N. H.; Amal, R.; Beydoun, D. *J. Photochem. Photobio. A-Chem.* **2006**, *179*, 57; and Niitsoo, O.; Sarkar, S. K.; Pejoux, C.; Ruhle, S.; Cahen, D.; Hodes, G. *J. Photochem. Photobio. A-Chem.* **2006**,

181, 306). However, the use of QDs to improve TiO_2 based solar cell efficiency is still an area of active exploration.

Hydrogen is very attractive as a clean fuel due to its high energy density and benign chemical byproduct, water (Bak, T.; Nowotny, J.; Rekas, M.; Sorrell, C. C. *Int. J. Hydrogen Energy* **2002**, 27, (10), 991-1022; Yilanci, A.; Dincer, I.; Ozturk, H. K. *Prog. Energ. Combust.* **2009**, 35, (3), 231-244). Producing hydrogen from water splitting using solar energy based on photoelectrochemical (PEC) cells, photovoltaic cells and photocatalysis is highly desirable because it leaves less of a carbon footprint and the resources used, water and sunlight, are abundant (Bak et al. *supra*; Yilanci et al. *supra*; Li, Y.; Zhang, J. Z. *Laser Photonics Rev.* **2009**, in press; Fujishima, A.; Honda, K. *Nature* **1972**, 238, (5358), 37-38; Heller, A. *Science* **1984**, 223, (4641), 1141-1148; Murphy, A. B. B., P.R.F.; Randeniya, L.K.; Plumb, I.C.; Grey, I.E.; Horne, M.D.; Glasscock, J.A. *Int. J. Hydrogen Energy* **2006**, 31, 1999-2017; Chen, D.; Gao, Y. F.; Wang, G.; Zhang, H.; Lu, W.; Li, J. H. *J. Phys. Chem. C* **2007**, 111, 13163-13169; Liu, J.; Cao, G.; Yang, Z.; Wang, D.; Dubois, D.; Zhou, X.; Graff, G. L.; Pederson, L. R.; Zhang J. G. *Chem. Sus. Chem.* **2008**, 1, 676-697; Khaselev, O.; Turner, J. A. *Science* **1998**, 280, (5362), 425-427; and Osterloh, F. E. *Chem. Mater.* **2008**, 20, 35-54). A conventional PEC cell is established with a semiconductor photoanode and a platinum electrode as the cathode in an electrolyte solution. Electrons and holes are created when a semiconductor anode absorbs light. The depletion layer formed at the semiconductor-electrolyte interface leads to energy band bending that facilitates separation of photogenerated electrons and holes. The electrons and holes perform chemical redox reactions at the semiconductor photoanode and the platinum cathode (Bak et al. *supra*; Fujishima and Honda *supra*). Typically, the reaction is the splitting of water, $2H_2O \rightarrow 2H_2 + O_2$, but hydrogen can also be generated by the use of sacrificial electrolytes, such as Na_2S and Na_2SO_3 (Rao, N. N.; Dube, S. *Int. J. Hydrogen Energy* **1996**, 21, (2), 95-98).

Wide bandgap semiconductors such as TiO_2, ZnO and WO_3 have been demonstrated as promising candidates for photoanodes due to their energy band position, thermal and chemical stability in solution (Bak et al. *supra*; Fujishima and Honda *supra*; and Yang, X.; Wolcottt, A.; Wang, G.; Sobo, A.; Fitzmorris, R. C.; Qian, F.; Zhang, J. Z.;

Li, Y. *Nano Lett.* **2009**, 9, (6), 2331-2336). However, they are not ideal due to their weak absorption of visible light (Murphy et al. *supra*). Doping of such wide bandgap metal oxides is one of the most promising approaches to increasing their visible light absorption. Asahi *et al.* first reported N-doped TiO_2 films prepared by sputtering that showed noticeable visible light absorption at wavelengths less than 500 nm due to the bandgap narrowing by mixing of N *2p* states with O *2p* states (Asahi, R.; Morikawa, T.; Ohwaki, T.; Aoki, K.; Taga, Y. *Science* **2001**, 293, (5528), 269-271). On the other hand, sensitizing metal oxides with small bandgap semiconductors is another attractive method for increasing their visible light absorption, which has recently been demonstrated for ZnO and TiO_2 (Tak, Y.; Hong, S. J.; Lee, J. S.; Yong, K. *Cryst. Growth Des.* **2009**, 9, (6), 2627-2632; Lee, Y. L.; Chi, C. F.; Liau, S. Y. *Chem. Mater.* **2009**, in press). When the conduction band edge of a small bandgap semiconductor is higher than that of the metal oxide, the photogenerated electrons in the small bandgap semiconductor can be injected to the conduction band of the metal oxide.

To date, both sensitization and doping of metal oxide nanostructures have been explored separately for solar energy conversion applications, yet little work has been done on combining the two approaches.

There is therefore a need in the art for compositions and methods for synthesis of hydrogen that is both relatively inexpensive and uses relatively simple compositions and components.

Summary of the Invention

The invention provides a thin film structure comprising a conducting substrate, a thin layer comprising nanocrystalline metal oxide doped with nitrogen thereon, and further comprising a semiconductor quantum dot and a linker thereon said thin layer of nanocrystalline metal oxide. In one preferred embodiment the conducting substrate is selected from the group consisting of indium tin oxide and fluorine tin oxide. In another preferred embodiment the nanocrystalline metal oxide is selected from the group consisting of titanium dioxide, tungsten oxide, and zinc oxide. In yet another preferred embodiment the semiconductor quantum dot is selected from the group consisting of

cadmium selenium and cadmium telluride. In a still further preferred embodiment the linker is selected from the group consisting of thioglycolic acid (TGA), mercapto-propanoic acid (MPA), and cysteine and links the semiconductor quantum dot with the conducting substrate.

The invention also provides a photovoltaic cell comprising the thin film structure as disclosed herein. In one preferred embodiment, the photovoltaic cell has a power conversion efficiency of between $1 \cdot 10^{-3}$ and 5 η%. In a more preferred embodiment the power conversion efficiency is of between $5 \cdot 10^{-3}$ and 1 η%. In another preferred embodiment the photovoltaic cell has an incident photon to current conversion efficiency (IPCE) of between 1% and 99.5%. In a more preferred embodiment, the IPCE is of between 13% and 95%. In a still further preferred embodiment the IPCE is of between 25% and 90%. In a yet further preferred embodiment the IPCE is of between 50% and 85%.

The invention further provides a hydrogen synthesis system comprising the photovoltaic cell comprising the thin film structure as disclosed herein. In one embodiment the hydrogen synthesis system further comprises hydrogen storage means wherein the hydrogen is stored therein. In a preferred embodiment the hydrogen storage means is selected from the group consisting of a cylinder, a tank, a gas tank, a vessel comprising a fluid in which the hydrogen is dissolved or dispersed under pressure, and the like. In another preferred embodiment, the hydrogen is stored as a phase selected from the group consisting of a gas, a liquid, and as a liquid or gas in a composition, the composition comprising a plurality of cavities, and the like.

The invention also provides a method for generating an electric current, the method comprising the steps of (i) providing a conducting substrate; (ii) doping a nanocrystalline metal oxide with nitrogen; (iii) depositing said crystalline metal oxide doped with nitrogen upon said conducting substrate; (iv) providing a semiconductor quantum dot; (v) linking said semiconductor quantum dot to said conducting substrate using a linker; (vi) irradiating the surface of said conducting substrate with a photon source thereby creating or inducing an electric current through the conducting substrate; the method thereby generating an electric current. In a preferred embodiment the photon source is selected from the group

consisting of a tungsten lamp, a fluorescent lamp, an arc lamp, a laser, a light-emitting diode, a liquid crystal diode, a radionuclide, the sun, a gamma ray, a fluorescent molecule composition, and the like. In one preferred embodiment the conducting substrate is selected from the group consisting of indium tin oxide and fluorine tin oxide. In another preferred embodiment the crystalline metal oxide is selected from the group consisting of titanium dioxide, tungsten oxide, and zinc oxide. In yet another preferred embodiment the semiconductor quantum dot is cadmium selenium and cadmium telluride. In a still further preferred embodiment the linker is selected from the group consisting of thioglycolic acid (TGA), mercaptopropanoic acid (MPA), and cysteine and links the semiconductor quantum dot with the conducting substrate.

In one embodiment the method herein disclosed comprises using a photon source wherein the photons from the photon source have power intensity of between 1 and 10000 mW/cm^2. In a preferred embodiment the photons from the photon source have power intensity of between 10 and 1000 mW/cm^2. In a more preferred embodiment the photons from the photon source have power intensity of between 25 and 250 mW/cm^2. In a yet more preferred embodiment the photons from the photon source have power intensity of 100 mW/cm^2. In an alternative more preferred embodiment the photons from the photon source have power intensity of 27 mW/cm^2. For example, the photons from the photon source can have a power intensity of 1, 2, 2.5, 3, 4, 5, 6, 7, 8, 9, 10, 12.5, 15, 17.5, 20, 25, 27, 30, 35, 40, 45, 50, 55, 60, 65, 70, 75, 80, 85, 90, 95, 100, 110, 120, 130, 140, 150, 160, 170, 180, 190, 200, 250, 300, 350, 400, 450, 500, 550, 600, 650, 700, 750, 800, 850, 900, 950, 1000, 2000, 3000, 4000, 5000, 6000, 7000, 8000, 9000, 10000 mW/cm^2 .

The invention also provides a method for generating hydrogen, the method comprising the steps of (i) providing a conducting substrate; (ii) doping a crystalline metal oxide with nitrogen; (iii) depositing said nanocrystalline metal oxide doped with nitrogen upon said conducting substrate; (iv) providing a semiconductor quantum dot; (v) linking said semiconductor quantum dot to said conducting substrate using a linker; (vi) providing a hydrogen source in contact with the opposing surface of said conducting substrate; (vii) irradiating the surface of said conducting substrate with a photon source thereby creating or inducing an electric current through the conducting substrate; (viii) allowing the electric

current to electrolyze the hydrogen source, thereby producing hydrogen; the method thereby generating hydrogen. In a preferred embodiment the photon source is selected from the group consisting of a tungsten lamp, a fluorescent lamp, an arc lamp, a laser, a light-emitting diode, a liquid crystal diode, a radionuclide, the sun, a gamma ray, a fluorescent molecule composition, and the like. In one preferred embodiment the conducting substrate is selected from the group consisting of indium tin oxide and fluorine tin oxide. In another preferred embodiment the nanocrystalline metal oxide is selected from the group consisting of titanium dioxide, tungsten oxide, and zinc oxide. In yet another preferred embodiment the semiconductor quantum dot is selected from the group consisting of cadmium selenium and cadmium telluride. In a still further preferred embodiment the linker is selected from the group consisting of thioglycolic acid (TGA), mercaptopropanoic acid (MPA), and cysteine and links the semiconductor quantum dot with the conducting substrate. In a preferred embodiment the hydrogen source is a compound comprising hydrogen, carbon, oxygen, or any combination thereof. In a more preferred embodiment the hydrogen source is selected from the group consisting of methanol, ethanol, water, formic acid, and an amine compound. For example, the hydrogen source can be an alcohol, an organic acid, or an organic waste compound, such as residual waste from households, commerce, and/or industry.

In one embodiment the method herein disclosed comprises using a photon source wherein the photons from the photon source have power intensity of between 1 and 10000 mW/cm^2. In a preferred embodiment the photons from the photon source have power intensity of between 10 and 1000 mW/cm^2. In a more preferred embodiment the photons from the photon source have power intensity of between 25 and 250 mW/cm^2. In a yet more preferred embodiment the photons from the photon source have power intensity of 100 mW/cm^2. In an alternative more preferred embodiment the photons from the photon source have power intensity of 27 mW/cm^2. For example, the photons from the photon source can have a power intensity of 1, 2, 2.5, 3, 4, 5, 6, 7, 8, 9, 10, 12.5, 15, 17.5, 20, 25, 27, 30, 35, 40, 45, 50, 55, 60, 65, 70, 75, 80, 85, 90, 95, 100, 110, 120, 130, 140, 150, 160, 170, 180, 190, 200, 250, 300, 350, 400, 450, 500, 550, 600, 650, 700, 750, 800, 850, 900, 950, 1000, 2000, 3000, 4000, 5000, 6000, 7000, 8000, 9000, 10000 mW/cm^2 .

Brief Description of the Drawings

Figure 1. Photovoltaic schematic of TiO_2:N-TGA-CdSe cells in (a) Na_2S electrolyte (b) solid. (c) Representation of TiO_2-3 and TiO_2-4 nanoparticles functionalized with CdSe linked with a bifunctional molecule TGA, in a porous film (using hexamethylenetetramine (HMT) and HMT+ polyethylene glycol (PEG) in the TiO_2 synthesis respectively). d) Representation of TiO_2-1-TGA-CdSe film (without nitric acid) and TiO_2-2-TGA-CdSe film (using nitric acid in the TiO_2 synthesis) with low porosity.

Figure 2. (a)) X-ray photoelectron spectroscopy (XPS) Spectra of nitrogen doped TiO_2-3 film on SnO_2:F substrate showing C, N, Ti, O and Sn spectra peaks. (b) A detailed N1s XPS band.

Figure 3. X-ray powder diffraction (XRD) patterns of TiO_2 films on the SnO_2:F substrate prepared by sol-gel method, using different chemicals in the TiO_2 synthesis, annealed at 550°C during 1.5h in a heat gun, for (a) TiO_2-1 film (without nitric acid), (b) TiO_2-2 film (using nitric acid), (c) TiO_2-3 film (using nitric acid and HMT) and (d) TiO_2-4 (using nitric acid, HMT and PEG). The phases found in the films are anatase, rutile and brookite marked by A, R and B respectively. SnF represents the crystal phase of the conductive glass (SnO_2:F).

Figure 4. TiO_2 films Raman Spectra of (a) TiO_2-1 (without nitric acid, HMT nor PEG), (b) TiO_2-3 (using nitric acid and HMT in the synthesis), (c) TiO_2-4 (using nitric acid, HMT and polyethylene glycol (PEG) in the synthesis).

Figure 5. Atomic force microscopy (AFM) images of (left) Nitrogen doped TiO_2-3 thin film (175 nm) and (right) N doped TiO_2-3 nanoparticles linked to TGA-CdSe nanoparticles (film thickness ~1100nm).

Figure 6. Representative transmission electron microscopy (TEM) image of CdSe quantum dots showing an average particle size around 3.5 nm.

Figure 7. UV-VIS absorption spectra of the films (a) TiO_2-1 (without nitric acid), (b) TiO_2-2 (using nitric acid in the synthesis without HMT), (c) TiO_2-3 film (synthesized with nitric acid and HMT), (d) TiO_2-4 film (synthesized with HMT and PEG) and (e) TiO_2-3 - TGA-CdSe film. The blank was the substrate of SnO_2:F (of the conductive glass).

Figure 8. UV-VIS absorption spectra of (a) CdSe nanoparticles and (b) Photoluminescence (PL) spectra of CdSe nanoparticles in toluene excited at 390 nm. (c) PL of TiO_2-3 film doped with nitrogen and sensitized with CdSe QDs.

Figure 9. I-V characteristic of (a) TiO_2-1-TGA-CdSe thick film, (b) TiO_2-3-TGA-CdSe thin film and (c) TiO_2-3-TGA-CdSe thick film. Using 1 M Na_2S, excited with halogen lamp with incident light intensity of $I_i = 27mW/cm^2$.

Figure 10. IPCE% of the different cells with (○) TiO_2-3 film without QD sensitization, (this curve is amplified 10x), (■) TiO_2-1-TGA-CdSe film with QD sensitization and (●) TiO_2-3-TGA-CdSe film with QD sensitization.

Figure 11. IPCE% of the solid state cell of TO_2-3-TGA-CdSe film in open air conditions. Inset is a UV-vis and PL spectra of CdSe QDs in toluene with an average size of 4.6 nm utilized to sensitize the nitrogen doped TiO_2-3 film.

Figure 12. Schematic electronic band structure of 3.5 nm CdSe with an effective bandgap of 2.17 eV and nanocrystalline TiO_2:N with a 3.2 eV bandgap, associated with normal TiO_2 and a N dopant state approximately 1.14 eV above the valence band; as reported by Asahi *et al* (as denoted by asterisk *; see Asahi, R.; Morikawa, T.; Ohwaki, T.; Aoki, K.; Taga, Y. *Science* **2001**, *293*, 269). Different electron and hole creation, relaxation, and recombination pathways are illustrated, including (A) photoexcitation of electron from the valence band (VB) to the conduction band (CB) of TiO_2, (B) transition or photoexcitation of electron from the N energy level to the CB of TiO_2, (C) recombination of electron in the CB of TiO_2 with hole in N energy level, (D) electron transfer or injection from the CB of CdSe QD to the CB of TiO_2, and (E) hole transfer from the VB of CdSe QD to the N energy level. Note that not all these processes can happen simultaneously and many of these are competing processes.

Figure 13. UV-VIS absorption spectra of TiO_2, TiO_2:N, CdSe-TiO_2 and CdSe-TiO_2:N nanoparticle films.

Figure 14. Linear sweep voltammograms collected from a) TiO_2; b) TiO_2:N; c) CdSe-TiO_2; and d) CdSe-TiO_2:N nanoparticle films, at a scan rate of 10 mV/s in dark and with light illumination of 100 mW/cm^2.

Figure 15. Proposed model for the electron transfer at CdSe/TiO_2 interface in a CdSe-TiO_2:N sample. All the energy levels are referenced to NHE scale. CB and VB are conduction band and valence band. Green lines and blue lines represent the energy levels of V_o and N_o respectively. The horizontal dashed line indicates H_2O/H_2 potential level. Red arrows highlight the hole and electron transfer from CdSe to TiO_2. Black dashed arrows highlight the possible electronic transitions between the different energy levels in TiO_2. The schematic diagram shows three possible competing pathways for the photogenerated holes in CdSe: (i) oxidization of S^{2-} to S_2^{2-}; (ii) recombination with electrons in the conduction band, and (iii) transfer to V_o levels in TiO_2.

Figure 16. Measured IPCE spectra of TiO_2, TiO_2:N, CdSe-TiO_2 and CdSe-TiO_2:N nanoparticle films in the region of 350 to 600 nm at a potential of 0 V vs. Ag/AgCl.

Figure 17. Linear sweep voltammograms collected at a scan rate of 10 mV/s from TiO_2, TiO_2:N, CdSe-TiO_2 and CdSe-TiO_2:N nanowire arrays, in dark and with light illumination of 100 mW/cm^2.

Figure 18. A general illustration of nanocrystalline TiO_2 doped with nitrogen deposited on an indium tin oxide (ITO) or fluorine tin oxide (FTO) conducting substrate. CdSe QD sensitization occurs via a linking molecule such as thioglycolic acid (TGA). Sunlight illustrated by the lightning bolts excites both the CdSe QDs as well as the TiO_2:N. Phtotogenerated electrons from CdSe are then injected into the TiO_2:N thin film and diffused to the backcontact as photocurrent.

Detailed Description of the Invention

In this disclosure, we demonstrate a relatively simple approach to dope TiO_2 nanoparticles with nitrogen and also efficiently sensitize the doped nanoparticles with CdSe quantum dots (QDs). The nanoparticle films have been characterized in terms of their structural, optical and morphological properties using a combination of experimental techniques. The results showed substantially enhanced photoresponse and high-energy conversion efficiency of the TiO_2 nanoparticle films when nitrogen doping and QD sensitization are used in unison. Possible explanations are provided in terms of the morphological and optical properties of the films. This method based on combined doping

and QD sensitization is promising for solid-state PV cells and photoelectrochemical applications.

We also disclose the synthesis and photoelectrochemical (PEC) studies of TiO_2 nanoparticles and nanowires simultaneously doped with nitrogen *and* sensitized with CdSe quantum dots (QDs). These novel nanocomposite structures have been applied successfully as photoanodes for PEC hydrogen generation using Na_2S and Na_2SO_3 as sacrificial reagents. We observed significant enhanced photoresponse in these nanocomposites compared to N-doped TiO_2 or CdSe QD sensitized TiO_2. The enhancement is attributed to the synergistic effect of CdSe sensitization *and* N-doping that facilitate hole transfer/transport from CdSe to TiO_2 through oxygen vacancy states (V_o) mediated by N-doping. The results demonstrate the importance of designing and manipulating the energy band alignment in composite nanomaterials for fundamentally improving charge separation and transport and thereby PEC properties.

The simultaneous application of nitrogen incorporation into nanocrystalline TiO_2 thin films along with CdSe quantum dot (QD/ nanoparticle) has shown to enhance photovoltaic performance and can be utilized also for photoelectrochemical (PEC) water splitting. While nitrogen doping of TiO_2 has been performed, and shown to increase visible light harvesting, it has never been used in conjunction with CdSe QD sensitization. The two-fold advantage of this system is that (1) nitrogen doping extends the absorption of TiO_2 to 600 nm into the visible range (without doping it is 380 nm) and (2) the CdSe QDs can be exploited to further collect light depending on the size of the nanocrystals into the TiO_2:N nanocrystalline thin film. A general illustration is given in Figure 19.

When considering the band structure of the nanocrystalline TiO_2:N in unison with the CdSe QDs, is where the unique aspects of this system arise. While it is well known that various dyes and QDs can inject electrons into the conduction band of nanocrystalline TiO_2 (Graetzel et al. *supra*), what is new in our system is the added benefit of the mid bandgap position of the nitrogen energy level (see Figure 12). One embodiment encompasses the energy bands associated with a 3.5 nm CdSe QD with a bandgap of 2.17 eV. Once photoexcited by a photon of greater energy than the bandgap, an electron-hole pair or exciton is generated. The electron now being in the conduction band of CdSe is

then injected into the conduction band of TiO_2:N (**D**) and the positive hole localized to the valence band. Photoexcited electrons in the conduction band of TiO_2:N then diffuse through the network of interconnected nanoparticles to generate a photocurrent. Other processes of photoexcitation and relaxation include arrows (**A, B** and **C**), which include excitation from the valence to conduction band of TiO_2:N (**A**), excitation from the nitrogen dopant energy level (**B**), and nonradiative recombination from the conduction band to nitrogen dopant level (**C**). Ultimately the most unique aspect of the doped and sensitized system is the ability for dopant level electrons from nitrogen to combine with valence band photogenerated holes. In most photovoltaic applications, hole mobility becomes the limiting factor for power conversion efficiency. The probablility of this pathway increases due to the localization of nitrogen doping on the surface of TiO_2:N and the conjugation of CdSe QDs through the TGA molecule.

Overall the performance of nitrogen doping of TiO_2 with sensitization of CdSe showed increased performance over simple CdSe sensitization of undoped TiO_2. Several types of TiO_2 thin films were produced with CdSe sensitization and during colloidal synthesis of the TiO_2, nitric acid was either not used or was used to acidify the solution to a pH= 1.23. TiO_2 thin films without and with nitric acid addition achieved power conversion efficiencies of 0.120 % and 0.729 %, respectively, when utilized with CdSe QD sensitization. Comparatively, when hexamethylenetetramine (HMT) was used as the nitrogen dopant source in conjunction with nitric acid addition and CdSe QD sensitization we were able to achieve a power conversion efficiency of 0.840 %, an increase of over 15 % what was seen without nitrogen doping. We believe this is due in large part to the electron recombination discussed above along with increased light absorption of the TiO_2:N in the visible region. While success has been definitively seen with the combination of both nitrogen doping and QD sensitization, we believe it can also be successfully applied to PEC cells as well for water splitting.

TiO_2 and TiO_2:N have both been shown to be able to split water and oxidize species on their surface photoelectrochemically. Our goal is to also extend this regime of work to include the two prong doping/sensitization protocol to produce hydrogen through photolysis. With increased photocurrents in the dual TiO_2:N-CdSe system we feel the

water splitting to be a natural progression from the characterization already performed in aqueous Na_2S solutions for photovoltaic applications.

1) Nitrogen Doped and CdSe Quantum Dot Sensitized Nanocrystalline TiO_2 Films for Solar Energy Conversion Applications

N-doping of TiO_2 nanoparticles with hexamethylenetetramine

It is known (Yin, S.; Komatsu, M.; Zhang, Q. W.; Saito, F.; Sato, T. *J. Mater. Science* **2007**, *42*, 2399) that hexamethylenetetramine (HMT) hydrolyzes in aqueous solutions to form ammonia and formaldehyde above 70 °C, as shown in the following equation:

$$C_6H_{12}N_4 + 6H_2O \xrightarrow{Hydrolysis} 6HCO + 4NH_3. \quad (1)$$

Ammonia reacts with $Ti(OCH(CH_3)_2)_4$ (TTIP) to form a nitrogen containing precursor ($TiO_{2-x}N_y \cdot nH_2O$). Dehydration of the TiO_2 complex in pure and doped TiO_2 samples is completed at temperatures below 200 °C and NH_3 molecules remain until the calcination temperature rises to 300 °C. Therefore, crystallization of $TiO_{2-x}N_y$ can be summarized as

$$TiO_2(TTIP) \xrightarrow{H_2O,NH_3,etc} TiO_{2-x}N_y \times nH_2O \xrightarrow{300^\circ C} TiO_{2-x}N_y. \quad (2)$$

A yellowish tint was observed in all films synthesized with HMT or HMT plus PEG, suggesting the presence of a TiO_2:N sol-gel solution (Livraghi et al. *supra*). The XPS spectra for all the films showed two evident peaks corresponding to Ti 2p, O 1s at 458.5 and 531.5 eV binding energies accompanying with traces of Sn from conductive SnO_2:F film over which the TiO_2 films were formed. Also traces of carbon at 284 eV were also present due to the intentional hydrocarbon contamination used for calibration. Carbon (C 1s) atoms percentage increases from 29% for *TiO_2-1* to 37% and 40% for *TiO_2-3* and *TiO_2-4* respectively. The *TiO_2-4* prepared with both HMT and PEG contains the highest carbon content, which may be attributed to uncombusted material from the precursor solutions, including HMT and PEG. The sample prepared with PEG, *TiO_2-4*, contains the

highest carbon content. Sample *TiO_2-2* prepared with nitric acid and without HMT in vacuum present extremely weak nitrogen signals at 401.2. However *TiO_2-3* and *TiO_2-4* films exhibit N 1s at ~400 eV and 401.2 eV, which are indicative of nitrogen incorporation. We attribute N 1s at 400 eV to N atoms from N-N, N-H, O-N or N-containing organic compounds absorbed on the surface. It has been reported that N 1s features appearing above 400 eV is due to Ti-O-N linkage suggesting that doping within the crystal lattice is in fact interstitial in nature (Moribe et al. *supra*).

Based on the XRD patterns of different TiO_2 films (Figure 3), nitric acid, HMT and PEG seem to have a significant effect on the TiO_2 crystalline structure. The phase composition appears to be strongly related to the added quantity of nitric acid, and therefore to pH. The film prepared without nitric acid shows pure anatase structure (Figure 3a). A reduction of the pH to 1.23 resulted in the appearance of rutile and brookite phases mixed with anatase (Figure 3b). However, for the samples prepared with HMT at pH~1.65, the antase phase decreases (Figure 3c). These results suggest that nitric acid and HMT promote the formation of brookite and rutile phases. The reason for this is not yet clear and needs further study. When added, PEG increases the pH to ~ 2.06, and the corresponding film shows a presence of the brookite and rutile phases (Figure 3d). Further research is also needed to understand the possible correlation between the different crystal phases and their photovoltaic performance.

The phases determined by XRD are supported by Raman scattering spectroscopy measurements of the films (Figure 4). The *TiO_2-1* thin film shows Raman peaks at 144, 399, 515 and 636 cm^{-1} (Figure 4a), which indicate a pure anatase crystal phase based on a previous report (Djaoued et al.). *TiO_2-3* thin film shows vibrational modes at about 244, 281, 409, 501, 589, and 633 cm^{-1}, indicative of the brookite phase, and peaks at 230, 445, and 604 cm^{-1}, indicative of a rutile phase. The *TiO_2-2* films contains a mixture of peaks that can be attributed to anatase, brookite, and rutile phases, as a result of nitric acid incorporation. The lowest frequency mode shifts slightly for these films to 146 cm^{-1} as compared to 144 cm^{-1} for the pure anatase (*TiO_2-1*). This might be caused by changes in crystallographic composition due to nitrogen doping attributed to the vibrations of Ti-N-O introduced by nitric acid and HMT. Raman spectrum of the *TiO_2-4* thin film shows that

PEG suppresses the formation of the rutile and brookite phases, also consistent with XRD data. The intensity of the 146 cm^{-1} peak for the *TiO_2-3* film is higher and sharper than undoped TiO_2, indicating good crystallinity and size uniformity of the TiO_2:N film.

Morphologic properties

Composition of the thin films was observed to be a mix of individual particles interconnected with high porosity. However, *TiO_2-3* and *TiO_2-4* films were far more porous than *TiO_2-1* and *TiO_2-2* films. This suggests that HMT and PEG promote porosity as was previously demonstrated in the case of PEG interacting with TiO_2 systems (Liu, X. X.; Jin, Z. G.; Bu, S. J.; Yin, T. *J. Sol-Gel Sci. Techn.* **2005**, *36*, 103). The morphology was noticeably more evident by AFM due to an atomically flatter surface produced with thin films on the order of 150 nm in thickness. The surface properties of the TiO_2:N films are expected to be important in determining how well the CdSe QDs can link to and interact with the TiO_2 nanoparticles. AFM images of all TiO_2 films functionalized with CdSe QDs clearly show the presence of QDs as evidenced by the apparent flattening of the films in the AFM images (for example, Figure 5 for the *TiO_2-3-TGA-CdSe* film).

Optical properties

Comparison of the absorption spectra of all samples under study show that films without HMT and PEG (*TiO_2-1* and *TiO_2-2*) have absorption around 340 and 400 nm respectively. However, *TiO_2-3* and *TiO_2-4* films with HMT or HMT plus PEG have a red shift of the absorption edge toward the visible region at 600 nm for samples annealed at 550 °C due to the electronic transition of N $2p_\pi$ to Ti d_{xy} (Figure 7c and 7d). The red-shift absorption can be attributed to the doping of nitrogen into the crystal lattice of TiO_2 due to the addition of HMT in the sol gel solutions. *TiO_2-3* and *TiO_2-4* films and calcined powders are also yellowish in color, attributed to the presence of nitrogen that results in the effective narrowing of the bandgap. All the films sensitized with CdSe QDs exhibit strong absorption at 560 nm, which is the characteristic excitonic absorption band of CdSe QDs (Figure 7e).

As shown in Figure 8, CdSe QDs in solution exhibit strong and narrow bandedge emission at 580 nm while the PL spectrum of the *TiO_2-3-TGA-CdSe* film shows a weak and blue-shifted PL band peaked at 575.5 nm. These results suggest interactions between TiO_2 nanoparticles and CdSe QDs and likely electron injection from CdSe to TiO_2. The small blue-shift of the PL peak could be due to slight oxidation of the film exposed to the atmosphere and thus a decrease in CdSe QD size during the sensitization process. The electron transfer process indicated by PL quenching is supported by photoelectrochemical measurements to be discussed later. *TiO_2-1* and *TiO_2-2* films also have emissions in 580 nm due to CdSe QDs. However, there is no blue-shift of the PL spectrum. This is possibly because the *TiO_2-1-CdSe* and *TiO_2-2-CdSe* have lower porosity than *TiO_2-3* and *TiO_2-4* and the CdSe QDs are not inside the pores of the TiO_2 film and thereby have weak interactions with TiO_2 nanoparticles. This is illustrated schematically in Figure 1d. The average QD size is estimated to be 3.5 nm based on the absorption spectrum.

Photoelectrochemical and photovoltaic characterization

As summarized in Table 1, thin and thick films sensitized with CdSe QDs show enhanced photocurrents and power conversion efficiency under white light, in comparison to films without sensitization of CdSe QDs. The greatest enhancement was observed for TiO_2 films doped with nitrogen and simultaneously sensitized with CdSe QDs. What is interesting is that the QD-sensitized TiO_2:N shows much larger enhancement than the simple sum of just N-doping and only QD sensitization, especially in terms of photocurrents (Figure 9). One possible explanation is that N-doping alters the surface property of the TiO_2 film so that the interaction between TiO_2 and CdSe QDs becomes stronger and allows for more efficient electron injection. XPS data also revealed a localization of nitrogen upon the surface (Figure 2b), and binding between exposed Cd^{2+} and surface nitrogen atoms on TiO_2 could also increase interaction The porosity of the TiO_2 film could also be affected by N-doping that in turn influences how the CdSe QDs enter the pores and adsorb on to the TiO_2:N nanocrystalline surface. The mixed brokite and rutile phases could also have some effect on the CdSe-TiO_2 interaction.

Table 1. Summary of the fill factor and power conversion efficiency results from our study of N-TiO_2-TGA-CdSe based solar cell in electrolyte (Na_2S). The power light was 27 mW/cm^2 (1/4 of AM1.5) equivalent irradiance.

Cell	$-I_{sc}$ ($\mu A/cm^2$).,	$-V_{oc}$, (V vs Ag/AgCl	$(JV)_{max}$ ($\mu A/cm^2 * V$)	Fill Factor (FF %)	Power Conversion Efficiency (η%)
			Thin films		
TiO_2-1	19	0.5	9.5	14.1	$4.96x10^{-3}$
TiO_2-3	19	0.7	13.3	14.5	$7.14x10^{-3}$
TiO_2-4	19	0.74	14.1	11.3	$5.88x10^{-3}$
TiO_2-3-TGA-CdSe	242	1.0	242	25.4	$2.28 x10^{-1}$
Thick films					
TiO_2-1	25	0.5	12.5	24	$1.11x10^{-2}$
TiO_2-1-TGA-CdSe	169	1.3	219.7	14.8	$1.20x10^{-1}$
TiO_2-2-TGA-CdSe	400	1.2	480	41	$7.29x10^{-1}$
TiO_2-3-TGA-CdSe	683	1.2	819	27.7	$8.40 x10^{-1}$
TiO_2-4-TGA-CdSe	390	0.62	241	10.37	$9.25x10^{-2}$

For the thick *TiO_2-1* and *TiO_2-2* films, it was also observed that a layer of CdSe QD film formed on the TiO_2 film surface. This seems to indicate that CdSe QDs did not all disperse into the pores of the TiO_2 films efficiently, and were instead localized upon the TiO_2 surface. Therefore, CdSe QDs inject electrons mainly in the TiO_2 film surface, with CdSe QDs in contact with a thin layer of TiO_2 nanoparticles, which could possibly explain why the short circuit current, FF, and conversion efficiency are low for these two films. However, the conversion efficiency of *TiO_2-2* is higher than that of *TiO_2-1*, probably due to nitrogen residues from the nitric acid added to TiO_2 sol.

In comparison to the thick *TiO_2-3-TGA-CdSe* film with the highest power conversion efficiency (η=0.84%), the *TiO_2-4-TGA-CdSe* (CdSe QD sensitized with HMT and PEG) has lower conversion efficiency. This could possibly be due to a weakened interaction between CdSe QDs and TiO_2 nanoparticles caused by hydrocarbon species on

the TiO_2 surface from uncombusted polyethylene glycol (PEG). It is clear that IPCE is enhanced when the films were sensitized with CdSe QDs (Table 2) due to their strong visible absorption and electron injection. The highest IPCE percentage was found for *TiO_2-3-TGA-CdSe* films (95% in 300 nm) where the larger content of brookite and rutile phases of the TiO_2:N was present. The lower IPCE in *TiO_2-1* samples is possibly due to the lower porosity and probably due to the presence of the anatase crystalline phase (Figure 10). The performance of the solid solar cell is similar to that reported previously, as shown in Figure 11 (Grant, C. D.; Schwartzberg, A. M.; Smestad, G. P.; Kowalik, J.; Tolbert, L. M.; Zhang, J. Z. *J. Electroanal. Chem.* **2002**, *522*, 40). In this case, the highest IPCE is 6% at 400 nm and a strong response, larger than 4%, was observed at 600 nm. The first increase at 600 nm is attributed to the absorption onset of the 4.6 nm QDs utilized to sensitize the *TiO_2*-3-TGA-CdSe film. The direct overlap with the first excitonic band (inset figure11) of the CdSe QDs with the IPCE measurements confirms the electron injection into the TiO_2 conductive band. This in turn, confirms the important role of the QDs to harvest photons and increase the generated photocurrent. All these results indicate the sensitive dependence of the cell performance on the film porosity, QD-TiO_2 interaction, and N-doping.

The electronic band structure of CdSe QD and TiO_2:N could help to better understand the reason behind increased performance in TiO_2:N thin films sensitized with CdSe. Figure 12 shows different electron-hole relaxation, recombination pathways and band structure of both CdSe QDs with a bandgap of 2.17 eV (3.5 nm in average diameter) and nitrogen doped TiO_2 with an overall bandgap of 3.2 eV at pH=7. The band diagram of CdSe and TiO_2:N have both been placed in relation to the normal hydrogen electrode (NHE). CdSe QDs of 3.5 nm has a top valence band position of ca. +0.7 V and a lower conduction band of ca. -1.4 V based on previous reports (Robel, I.; Subramanian, V.; Kuno, M.; Kamat, P. V. *J. Am. Chem. Soc.* **2006**, *128*, 2385). The band structure of TiO_2:N in turn has a valence band at ca. +2.6 V and a conductive band at ca. -0.6 V based on the work by Sakthivel and Kisch (Sakthivel, S.; Janczarek, M.; Kisch, H. *J. Phys. Chem. B* **2004**, *108*, 19384; Sakthivel, S.; Kisch, H. *Chemphyschem* **2003**, *4*, 487). N doping introduces a state at 1.14 eV above the valence band and 2.06 eV (600 nm

absorption onset) below the conduction band of TiO_2 (Di Valentin et al. *supra*). Several groups have also reported an absorption onset at 600 nm via reflectance spectroscopy Chen, X. B.; Burda, C. *J. Phys. Chem. B* **2004**, *108*, 15446; (Burda, C.; Lou, Y. B.; Chen, X. B.; Samia, A. C. S.; Stout, J.; Gole, J. L. *Nano Letters* **2003**, *3*, 1049; and Gole, J. L.; Stout, J. D.; and Burda, C.; Lou, Y. B.; Chen, X. B. *J. Phys. Chem. B* **2004**, *108*, 1230). Incorporation of nitrogen into nanocrystalline TiO_2 acts as an electron acceptor site within the TiO_2 bandgap, and effectively should be considered a p-type doping. This state acts as an electron acceptor site within the TiO_2 bandgap. Now it is still important to consider the typical n-type behavior of TiO_2 as a result of oxygen vacancies in the crystal lattice, and therefore act as donor sites within the structure, and effectively increase the Fermi level (E_f) to more negative potentials (versus NHE). The bandgap dopant N state is populated as evidenced by the weak absorption onset at 600 nm (2.06 eV) explained by Asahi *et al.* (2001, *supra*) as a N $2p_{\Pi}$ to Ti d_{xy} transition. Due to the relatively weak absorption of this N $2p_{\Pi}$ to Ti d_{xy} electronic transition in comparison to the quantum confined CdSe transition ($1S_h1S_e$) transition, we expect that, for the CdSe QD sensitized TiO_2:N films, the optical absorption is dominated by the CdSe QDs.

To understand the charge transfer and recombination kinetics, we will ignore the weak absorption due to N-doping for the QD sensitized TiO_2:N film. In this case, photoexcitation of the CdSe QD generates a hole in its valence band and an electron in its conduction band. The electron in the conduction band of CdSe QD is injected into the conduction band of TiO_2 (left to right yellow arrow) and the transfer of the hole in the valence band of CdSe can be mediated by the electron occupied N state (right to left yellow arrow). The energy level of the N state is close to the top of the valence band of CdSe and this proximity in energy will aid in the hole (or electron) transfer process. Since this only exists for the CdSe QD sensitized and N-doped TiO_2 film, the N-mediated hole transport may be the key to the enhanced photoelectrical response of this film compared to TiO_2 films with only N doping or only QD sensitization. This is possible, especially considering that the hole transport is often the limiting step for overall charge transport in nanoparticle films.

It is clear that N doping into TiO_2 has introduced extra pathways for the charge carriers that could be beneficial for overall chare transport and thereby cell performance. Optimization of the system via an increased dopant level (currently 0.6-0.8 %, see Table 1) and manipulation of the capping agents of CdSe may further enhance the photocurrent density as well as power conversion efficiency above that of 0.84% currently observed.

Conclusions

Several TiO_2 films with nitrogen doping and/or CdSe QD sensitization have been systematically investigated using a combination of synthetic, spectroscopic, XRD, XPS, microscopy, and electrochemistry techniques. The structure of TiO_2:N has been found to be generally a mixture of anatase, brookite, and rutile phases. Nitrogen doping into the TiO_2 lattice results in a red-shift of the electronic absorption and enhanced photocurrent response of relative to undoped TiO_2 films. In addition, CdSe QDs linked to TiO_2:N nanoparticles were found to significantly increase the photocurrent and power conversion of the films compared to standard TiO_2:N films without QD sensitization. The IPCE is 6% at 400 nm for TiO_2:N-TGA-CdSe solid state solar cells and 95% for TiO_2:N-TGA-CdSe films near 300 nm in a Na_2S electrolyte, which is much higher than undoped TiO_2 with QD sensitization or TiO_2:N without QD sensitization. A power conversion efficiency (η) of 0.84% was found along with a fill factor (FF%) of 27.7% for 1100 nm thick TiO_2:N-TGA-CdSe thin films. The results show that the combination of nitrogen doping and QD sensitization of TiO_2 thin films is an effective way to enhance the photoresponse, which is promising for photovoltaic (PV) and photoelectrochemical applications.

One exemplary application comprises a photovoltaic cell comprising the thin film structure as disclosed herein. In one embodiment, the photovoltaic cell has a power conversion efficiency of between $1 \cdot 10^{-3}$ and 5 η%. In another embodiment the power conversion efficiency is of between $5 \cdot 10^{-3}$ and 1 η%. For example, the power conversion efficiency can be $1 \cdot 10^{-3}$, $2.5 \cdot 10^{-3}$, $5 \cdot 10^{-3}$, $1 \cdot 10^{-2}$, $2.5 \cdot 10^{-2}$, $5 \cdot 10^{-2}$, $1 \cdot 10^{-1}$, $2.5 \cdot 10^{-1}$, $5 \cdot 10^{-1}$, 1, 1.5, 2, 2.5, 3, 3.5, 4, 4.5, and 5 η%.

In another embodiment the photovoltaic cell has an incident photon to current conversion efficiency (IPCE) of between 1% and 99%. In another embodiment, the IPCE

is of between 13% and 95%. In another embodiment the IPCE is of between 25% and 90%. In yet another embodiment the IPCE is of between 50% and 85%. For example, the IPCE can be 1%, 2%, 5%, 7.5%, 10%, 12.5%, 15%, 17.5%, 20%, 25%, 30%, 35%, 40%, 45%, 50%, 55%, 60%, 65%, 70%, 75%, 80%, 85%, 90%, 95%, 96%, 97%, 98%, 99%, and 99.5%.

2) Synergistic Effect of CdSe Quantum Dot Sensitization and Nitrogen Doping of TiO_2 Nanostructures for Photoelectrochemical Applications

Our lab has demonstrated a synergistic effect in combining CdSe QD sensitization with N-doping of TiO_2 that substantially increases photovoltaic response and was tentatively attributed to increased hole transport from the CdSe valence band to the N dopant level (Lopez-Luke et al. *supra*). In this work, we report the first example of CdSe QD sensitized *and* N-doped TiO_2 nanomaterials for PEC hydrogen generation with substantially enhanced photocurrent. Again, significant synergistic effect between QD sensitization and N-doping has been observed. A detailed study reveals that it is still the enhanced hole transfer/transport that is responsible for the observed synergistic effect, however, the enhanced hoe transfer/transport is not directly coupled to the N energy levels but is rather caused by oxygen vacancy states (V_o) of TiO_2 that is mediated indirectly by N-doping.

We have synthesized novel nanocomposite materials based on visible light-absorbing CdSe QDs and N-doped TiO_2 nanoparticles and nanowire arrays with properties tailored for PEC hydrogen generation. We have experimentally demonstrated for the first time, to our best knowledge, that the synergistic effect of sensitization *and* elemental doping significantly enhances the photoelectrochemical activities of the TiO_2 nanostructured photoanodes. These composite nanostructures show enhanced overall charge transport and improved PEC performance when the relevant bandgap states are properly aligned and utilized. Enhanced electron-hole separation and hole transfer/transport through the oxygen vacancy states, V_o, mediated by N-doping has been proposed to explain the observed experimental results. Such nanocomposite structures simultaneously enhance visible light absorption and interfacial charge transfer. The results

provide useful insights for developing new nanostructures tailored for PEC and other applications via controlled band engineering.

The invention will be more readily understood by reference to the following examples, which are included merely for purposes of illustration of certain aspects and embodiments of the present invention and not as limitations.

Examples

Example I: Experimental Sample Preparation

A. Materials.

Titanium(IV) iso-propoxide (#377996, 99%), technical grade trioctylphosphine (TOP-#117854, 90%), trioctylphosphine oxide (TOPO # 223301, 99%) , potassium chloride (KCl-#204099 , 99%), polyethylene glycol (PEG-#25322-68-3, average M_n ca. 10,000 g/mol) and sodium sulfide (Na_2S-# 407410, 99%) were obtained from Sigma-Aldrich (Milwaukee, WI.). Cadmium oxide (CdO-# 223791000, 99%) and selenium powder (Se 200 mesh-#198070500, 99%) were obtained from Acros organics (Morris Plains, NJ). 1-tetradecylphosphonic acid (TDPA-# 4671-75-4, 99%) was obtained from PCI synthesis (Newburyport, MA). Nitric acid (2.0N-#LC178502) was purchased from Lab. Chem Inc (Pittsburgh, PA). Thioglycolic acid (TGA-#103036, 98%) was obtained from MP Biomedicals Inc.(Solon, OH). F:SnO_2 conductive glass (Tec glass 30 Ohms) was obtained from Hartford glass (Hartford City, IN) and the reference electrodes Ag/AgCl from CH Instruments Inc. (Austin, TX).

B. TiO_2 film preparation.

Four kinds of TiO_2 films (*TiO_2-1*, *TiO_2-2*, *TiO_2-3* and *TiO_2-4*) were made by a sol-gel method. All TiO_2 films were made using 375 µL of titanium iso-propoxide as a precursor which was stored in a nitrogen filled glovebox. For TiO_2-1, TiO_2-2, TiO_2-3 and TiO_2-4, titanium iso-propoxide was injected into 250 µl of Milli-Q water and 5 mL of ethanol within the glovebox. *TiO_2-1* solutions did not contain nitric acid, while *TiO_2-2* solutions contained a drop wise addition of nitric acid until the solution reached a pH ~ 1.23. *TiO_2-3* solutions is similar to TiO_2-2, but 0.05 g of HMT was added under vigorous

stirring. Solution *TiO_2-4* is similar to TiO_2-3 with an addition of 0.90 g of polyethyleneglycol (PEG-10,000 g/mol) under vigorous stirring all within an O_2 free environment. As a point of clarification, acidification (TiO_2-2, TiO_2-3 and TiO_2-4) was performed outside of the glovebox prior to titanium isopropoxide addition within the glovebox. The sol was then stirred for three days within the glovebox at ambient temperatures (~ 25 °C). All TiO_2 films were made by spin coating at 2000 rpm for 60 seconds onto FTO (SnO_2:F) conducting substrates in ambient conditions. The thickness was estimated with mass, area and density of the TiO_2 films and was confirmed with AFM measurements (~150 nm and ~1100 nm thick). The films were annealed at 550 °C for 1.5 hours with a Leister heat gun in open air conditions. For thin TiO_2-1, TiO_2-2, TiO_2-3 and TiO_2-4 films, 50, 200, 100 and 50 μL of the sol solution was used, respectively. For thick TiO_2-1, TiO_2-2, TiO_2-3 and TiO_2-4 films, 400, 2000, 700, 250 μL respectively of the sol solution was used. The sol solution was put on the conductive glass with 1×2.2 cm^2 areas, respectively. It was necessary to apply different volumes in order to obtain approximately the same film thickness because of the different viscosities of the various solutions.

C. CdSe QD synthesis.

High-quality CdSe QDs were synthesized based upon the protocol of Qu, Peng, and Peng (2001) wherein CdO is utilized as the Cd precursor, and TDPA and TOPO are the ligands and coordinating solvents, respectively (see Qu, Peng, and Peng, *Nano Letters* **2001**, *1*, 333). The resulting CdSe nanocrystals were in the strong confinement size regime and were synthesized in normal air-free reaction conditions. The synthesis of the CdSe nanoparticle follows the procedure reported by Robel *et al.* wherein 0.05 g (~0.39 mmol) CdO, 0.3 g (~1.1 mmol) TDPA and 4 g of TOPO was heated to 110 °C and degassed under vacuum and then heated to 300 °C under a nitrogen flow (Schlenk line) (Robel et al. *Am. Chem. Soc.* **2006**, *128*, 2385). A SeTOP (0.7% by weight) solution was obtained by adding 0.026 g of Se powder with 4.25ml of TOP inside a glove box and stirred for 1hr to insure complete dissolution of the Se powder. After reaching 300 °C the Cd-TDPA-TOPO solution was cooled to 270 °C prior to the injection of SeTOP. Under a nitrogen flow, 3 ml of SeTOP was injected, which resulted in the lowering of the temperature to 260 °C. The temperature was then increased to 280 °C to facilitate particle growth and aliquots were

removed and probed to track nanocrystallite growth via UV-vis absorption spectroscopy and photoluminescence (PL) spectroscopy. The CdSe solution was cooled and was removed from the reaction flask at around 80 °C and dissolved into ~ 10 mL of toluene. The QDs in toluene were then cleaned twice through a precipitation and decantation regime using methanol and centrifugation at 3000 rpm, and the QDs were ultimately redissolved in toluene prior to their use as a sensitizer.

D. CdSe QD linkage to TiO_2.

CdSe QDs were linked to nanocrystalline TiO_2 and TiO_2:N thin films using TGA as a molecular linker. TiO_2 has a strong affinity for the carboxylate group of the linker molecules, while the sulfur atom of TGA binds strongly to CdSe nanoparticles through surface Cd^{2+} cations. The films were heated in a heat gun at 100 °C for 4 hrs to remove H_2O from the surface due to ambient humidity adsorption. They were later immersed in undiluted neat TGA for 12 hrs in a nitrogen environment in a glove box. The films were then immersed in toluene, removing the excess TGA and in turn immersed in a CdSe solution for 12 hrs inside the glove box. Four films of 1×1 cm^2 were immersed in 5 ml of CdSe QDs suspended in toluene as described earlier. The TiO_2:N-TGA-CdSe films were stored in a nitrogen filled glove box and not exposed to light prior to PEC characterization. The solid state TiO_2:N-TGA-CdSe cell after PEC measurements remained stable for months . The TiO_2:N-TGA-CdSe cell in the electrolyte is very stable, however, when is removed from the electrolyte the PEC properties diminish after a hours of experimentation. Long term stability need to be further studied in future research.

Example II: Structural and morphology characterization

X-ray photoelectron spectroscopy (XPS) studies of the films were carried out on an X-ray photoelectron spectrometer (XPS, PHI Quantera SXM) using a non-monochromatized Al KR X-ray source (1486.6 eV). The energy resolution of the spectrometer was set at 0.5 eV. The binding energy was calibrated using a C 1s (284.6 eV) spectrum of a hydrocarbon that remained in the XPS analysis chamber as a contaminant. Crystalline phase identification was performed via X-ray diffraction (XRD) in conjunction

with Raman spectroscopy. XRD analysis was conducted on a MINIFLEX diffractometer operating at 30 kV/15 mA using Cu-Kα radiation and scanning speed of 1° 2θ/min.

Raman spectroscopy of the films was performed using a Renishaw micro-Raman setup with a (5/ 10/ 20/ 50) X objective lens and a 633 nm excitation wavelength. Renishaw's WiRE (Windows based Raman Environment) was used for collection and data analysis of 1 to 5 scans ranging in accumulations of 1 to 10 seconds.

AFM images of the films without and with QDs were acquired under ambient conditions with a PicoLE SPM instrument (Molecular Imaging) in tapping mode. The tapping mode cantilevers exhibit resonant frequencies between 60 and 90 kHz (typical 75 kHz), force constants of 2.5-5.5 N/m, and tip apex radii of ~10 nm. The resulting images were flattened and plane-fit using software from Molecular Imaging. Silica etched tips were purchased from MikroMasch (Watsonville, OR).

A JEOL model JEM-1200EX microscope was used for the low-resolution transmission electron microscope (TEM) studies of the CdSe QDs. The TEM was equipped with a Gatan Model 792 Bioscan digital camera running on a Windows 2000 computer with Gatan Digital Micrograph as the analyzing software.

Example III: Optical and electrochemical characterization

UV-visible light (UV-vis) absorption spectroscopy was conducted on a Hewlett-Packard 8452A diode array spectrophotometer. UV-vis absorption spectra were measured first by placing a blank FTO glass substrate in the light path, subtracting the absorption pattern, and then performing the UV-VIS absorption measurement on the variety of TiO_2 thin films.

Photoluminescence (PL) spectroscopy was gathered on a Perkin Elmer LS 50B with an excitation wavelength of 390 nm and 1% attenuator. QDs in toluene were placed in an open sided 1 cm path length quartz cuvette for both UV-vis absorption and PL measurements. Thin films were placed in a thin film sample holder from Perkin Elmer (#52123130) for PL spectra.

Photoelectrochemical studies (linear sweep voltammetry and incident photon-to-current conversion efficiency (IPCE) in solid state and in electrolyte were carried out with

a CHI440 electrochemical workstation (Austin, TX). Linear sweep voltammetry was used to obtain the I-V profiles. Actively investigated thin films were the TiO_2, TiO_2:N and TiO_2:N-CdSe thin films described earlier. A Ag/AgCl and Pt wire coil were used as reference and counter electrodes, respectively. Before each measurement the Na_2S electrolyte solution was deaerated by bubbling ultra-high-purity N_2 for 20 minutes through the electrolyte solution and a nitrogen flow was also subsequently blown over the surface during data gathering. For I-V measurements a halogen lamp was utilized (75 watts) and for IPCE measurements and a 1000W Xe lamp (Oriel Research Arc Lamp assembly #69924 and power supply #69920) coupled to a infrared (IR) water filled filter (Oriel # 6127), and then aligned into a monochromator (Oriel Cornerstone 130 1/8m) for spectral resolution from 300 to 800 nm,. An aqueous Na_2S solution serves as the redox couple to maintain the stability of the QD's, as discussed elsewhere (Mueller, N.; Tenne, R.; Cahen, D. *J. Electroanal. Chem.* **1981**, *130*, 373; Ueno, Y.; Minoura, H.; Nishikawa, T.; Tsuiki, M. *J. Electrochem. Soc.* **1983**, *130*, 43). A maximum photocurrent was produced with 1 M Na_2S using 6.5 ml of Milli-Q water (18 MΩ). Diminished molarities of Na_2S were found to decrease overall photocurrent performance. IPCE measurements were also conducted for solid state TiO_2:N-TGA-CdSe solar cells. A schematic of the photoelectrochemical setup is shown in Figure 1(a-b).

Example IV: Results

The amount of nitrogen in N-doped TiO_2 nanoparticle films was identified by the XPS technique. Figure 2 shows the XPS spectra for the *TiO_2-3* film. Figure 2a shows the Ti2p, O1s, C1s, N1s and Sn binding energy from 0 to 1000 eV (Sn is identified from the conductive film). Figure 2b shows only the nitrogen binding energy from 396 to 408eV, showing two peaks at 400 and above 401.2eV. To compare the effect of HMT and PEG, *TiO_2-3* film has 37.45 % of C, 0.60 % of N, 50.16 % of O and 11.79 % of Ti. *TiO_2-4* film shows elemental composition of C and N of 39.93% and 0.80%, respectively, with 48% of O and 11.27 % of Ti.

Figure 3 shows the XRD patterns for all the films prepared, respectively, for determining the crystal phases of both TiO_2 and TiO_2:N. All the XRD data show the

crystal phase of the conductive glass (SnO_2:F), which is marked as (SnF). The *TiO_2-1* film (without nitric acid) XRD pattern is representative of the anatase crystal phase (Figure 3a). For the *TiO_2-2* film (with nitric acid), the brookite and rutile phases appear, with a mix of anatase, brookite and rutile phases (Figure 3b). With HMT added for the *TiO_2-3* film, a mixture of brookite and rutile phases dominate with a trace amount of anatase phase (Figure 3c). With further addition of PEG and HMT, as in the *TiO_2-4* film, the brookite and rutile phases decrease and the anatase is predominant. Additional evidence for the various crystal phases of the different films comes from their Raman spectra that show anatase as the primary phase for *TiO_2-1* and *TiO_2-4*, (Figure 4a and 4c) and a mix of anatase, brookite and rutile phases in *TiO_2-2* and *TiO_2-3* films. Representative Raman spectrum of the *TiO_2-3* film is shown in Figure 4b. It can be seen that the characteristic peak for the anatase phase at 144 cm^{-1} shifts slightly to 146 cm^{-1} with nitrogen doping (*TiO_2-3* and *TiO_2-4 films*).

Morphology of the films with and without QDs was studied by AFM in ambient conditions. The average TiO_2 nanocrystal size was found to be around 100 nm in diameter. Films with HMT (*TiO_2-3*) or HMT plus PEG (*TiO_2-4*) show more porosity than *TiO_2-1* and *TiO_2-2* films. A representative AFM image for the *TiO_2-3* film with about 150 nm thickness is shown in Figure 5a. For thicker films (for example, 1100 nm), TiO_2 particles were observed to form clusters. All films show the presence of CdSe QDs after they were sensitized, as exemplified by the AFM image for the *TiO_2-3-TGA-CdSe* film shown in Figure 5b. While it is not easy to determine the exact size of the CdSe QDs based on AFM, the average size of the QDs appear to be on the order of a few nanometers. To better characterize the CdSe QDs, TEM measurements was conducted. Figure 6 shows a representative TEM image of CdSe QDs. The image appears to show reasonably uniform size distributions of the CdSe QDs with an average diameter of 3.5 nm.

Optical absorption of the different films was characterized by UV-Vis spectroscopy, with emphasis on comparing the effect of nitrogen doping through HMT or nitric acid. Figure 7 shows a comparison of the UV-vis absorption spectra of different films. For films without HMT and PEG (*TiO_2-1* and *TiO_2-2*), the absorption is primarily around 340 and 400 nm (Figure 7a and 7b). However, for films with HMT (*TiO_2-3* and

TiO_2-4), the spectra show an obvious red-shift of the absorption edge towards the visible region, with peaks around 350, 426, and 542 nm (Figure 7c) or 412 nm, 532 nm and an absorption onset at 600 nm (Figure 7d). Figure 7e shows the UV-vis absorption spectrum of the TiO_2-3-CdSe film, with strong absorption around 560 nm due to the CdSe QDs. For comparison, Figure 8a and 8b show the absorption and photoluminescence (PL) spectra of CdSe QDs in toluene under ambient conditions. The absorption spectrum shows the expected strong and sharp excitonic peak around 560 nm while the PL spectrum shows a narrow emission band near 580 nm, which is clearly due to bandedge emisison. Figure 8c shows the PL spectrum of the *TiO_2-3-TGA-CdSe* film, with a relatively weak emission peak at 575.5 nm, which is slightly blue shifted with respect to the PL peak of CdSe QDs in toluene solution.

The current-voltage (I-V) profiles for solar cells fabricated using the films with different thicknesses (150 nm and 1100 nm) were obtained using a halogen lamp and a 1 M Na_2S. With the cell configuration shown schematically in Figure 1, the I-V profiles measured are shown in Figure 9. The cell without HMT (*TiO_2-1-CdSe* film) present a low short-circuit current density of -169 $\mu A/cm^2$ with an open-circuit voltage of -1.3V (Figure 9a) within the voltage window of -1.4 to 0.3 V, and the fill factor is 14.8% with a low power conversion efficiency of η=0.120%. For the cell based on *TiO_2-3-TGA-CdSe* thin film (150 nm), the I-V curve in Figure 9b shows a short-circuit current (-242 $\mu A/cm^2$) with an open-circuit voltage of -1.0 V, a fill factor of 25.4% and power efficiency of η=0.228%. The cell based on *TiO_2-3-TGA-CdSe* thick film (1100 nm) have the highest short-circuit (-683 $\mu A/cm^2$) with an open-circuit voltage of 1.2V (Figure 9c) and the highest fill factor of 27.7% and power conversion efficiency of η=0.840%. Short-circuit current and open circuit voltage found in Figure 9 is summarized in Table 1.

The fill factor (*FF*) and power conversion efficiency (η%) were calculated using short-circuit current and open circuit voltage[45] and are also given in Table 1.

$$FF=(jV_{max})/(j_{sc}\,V_{oc}) \quad (3)$$

$$\eta=(jV_{max})/I_i=FF\,(j_{sc}\,V_{oc})/I_i \quad (4)$$

where j_{sc} is the short circuit current density, V_{oc} is the open circuit voltage, $(jV)_{max}$ is the maximum power observed from the current density-voltage curve for each device and I_i is the incident light power density (27 mW/cm^2). It is clear that thick films (~1100 nm) exhibit a higher FF and η% than thin films (~150 nm). However, cells with TiO_2:N nanoparticles sensitized with CdSe QDs exhibit a much higher η% than films without sensitization.

The incident photon to current conversion efficiency (IPCE) was studied for solid cells and in electrolyte (1M Na_2S) with different thicknesses. IPCE at different wavelengths was determined from the short circuit photocurrent (j_{sc}), where $V=0$ at different excitation wavelengths (λ) using the expression:

$$\text{IPCE } \% = [(1240 \times j_{sc}(\text{A/cm}^2)]/ [\lambda(\text{nm}) \times I_i(\text{w/cm}^2)] \times 100 \qquad (5)$$

where I_{inc} is the incident light power. The IPCE results of TiO_2 and TiO_2:N without and with CdSe QDs are shown in Figure 10. It is clear that the photocurrent response is much stronger with the presence of CdSe QD sensitization. The *TiO_2-1-TGA-CdSe* film (QD sensitized but without N doping) shows photocurrent responses at 300, 530 and 620 nm, with the highest response near 300 nm with IPCE=56%. The *TiO_2-3-TGA-CdSe* film (QD sensitized and N-doped) shows similar response but an overall stronger IPCE with the highest response around 95% at 300 nm. The IPCE of both films closely match the absorption spectrum of CdSe QDs, and TiO_2:N as shown in Figure 7e. The IPCE% is 1.06 at 300nm for TiO_2:N (magnified 10X in Figure 10) showing photocurrent responses at 320, 360 and 420 nm also which are close to absorption spectrum as shown in Figure 7c.

In addition, the IPCE% of *TiO_2-3-TGA-CdSe* thin film (150 nm) solid cell was studied and the result is shown in Figure 11. It can be seen that peaks at 480 and 600 nm correspond to absorption of the CdSe QDs (see Figure 11 inset that shows the absorption and emission spectra of the CdSe nanoparticles in toluene). This cell shows an IPCE response around 6% at 400 nm and the results are summarized in Table 2.

Table 2 Summary of IPCE results from our study of thin and thick films based solar cell in electrolyte (Na_2S) and solid state. Was used a Xenon lamp (1000Watts) varying the wavelength with a monochromator.

Film type	IPCE% (300nm)
TiO_2-1-CdSe Thick film	56
TiO_2-2-CdSe Thick film	65
TiO_2-3-CdSe Thick film	95
TiO_2-4-CdSe Thick film	53
TiO_2-4-CdSe Thin film	2.5
TiO_2-3 Thick film	1.06
TiO_2-3-CdSe Thin (solid)	6 (400nm)

Example V: Synthesis and Analysis of Nanoparticle Films and Nanowires

To understand the synergistic effect between N-doping *and* CdSe sensitization, we synthesized and studied the PEC properties of both anatase TiO_2 nanoparticle films and vertically aligned rutile TiO_2 nanowire arrays. TiO_2 nanoparticle films were made by spin coating 150 μL of TiO_2 sol-gel nanoparticle solution at 2000 rpm for 1 minute on a piece of fluorine-doped tin oxide (FTO) conductive glass. The films were dried at 50 °C for 30 minutes, followed by repeated coating and drying, and eventually sintered in air at 550 °C, as previously described (Guo, B.; Liu, Z.; Hong, L.; Jiang, H.; Lee, J. Y. *Thin Solid Films* **2005**, 479, (1-2), 310-315). TiO_2 nanowire arrays were grown on FTO glass based on a recently reported hydrothermal method with slight modification (Liu, B.; Aydril, E. S. *J. Am. Chem. Soc.* **2009**, 131, 3985-3990). The FTO substrate was placed in a Teflon-lined stainless steel autoclave consisting of a mixture of aqueous solution of titanium n-butoxide

and hydrochloric acid. The autoclave was heated in an electric oven at 150 °C for 5 hours, and a uniform film of dense and vertically aligned TiO_2 nanowire arrays on a substrate was obtained. N-doping of the nanomaterial films was achieved by annealing in an ammonia atmosphere at 530 °C using a quartz tube furnace (Yang et al. *supra*). Films were sensitized with CdSe QDs by chemical bath deposition (CBD) following previously published results (Kale, R. B.; Lokhande, C. D. *J. Phys. Chem. B* **2005**, 109, (43), 20288-20294). A concentrated ammonia solution was added to 10 ml of 0.5 M aqueous solution of $Cd(acetate)_2$ dihydrate to a pH of 12.5 followed by the slow addition of 30 ml of 0.25 M Na_2SeSO_3 while being stirred for a few minutes. TiO_2 films were placed vertically in the solution at room temperature for about 15 hours to allow deposition of CdSe onto TiO_2.

The resulting TiO_2 nanoparticle films were characterized using electron microscopy and spectroscopy techniques. Scanning electron microscopy (SEM) studies verified that the sintered TiO_2 nanoparticle film has good coverage of the substrate, with a thickness of ~200 nm. Atomic force microscopy studies confirmed that the film is porous with particles ~50-100 nm in size. X-ray power diffraction results proved that the sintered TiO_2 nanoparticles have anatase crystal structures. More importantly, there is no phase change after annealing the nanoparticle films in ammonia. After ammonia annealing, the color of the TiO_2 nanoparticle films changed from colorless to pale yellow, suggesting that the incorporation of N introduces bandgap states of TiO_2 and thereby enhances visible light absorption.

To gain a quantitative understanding on the concentration and chemical state of the doped N, we performed X-ray photoelectron spectroscopy (XPS) analysis of the TiO_2 nanoparticle films. High resolution XPS spectrum of the N 1s region showed three peaks centered at 402.4 eV, 400.0 eV and 397.2 eV respectively. The peaks located at 402.4 eV and 400.0 eV can be ascribed to chemisorbed N_2 and/or amines (NH_x) originating from ammonia annealing (Asahi et al. *supra*; Saha, N. C.; Tompkins, H. G. *J. Appl. Phys.* **1992**, 72, (7), 3072-3079). The peak at 397.2 eV is typical of the N 1s binding energy of oxynitride (O-Ti-N), confirming that atomic N atoms incorporate substitutionally at O sites (Vitiello, P. R.; Macak, J. M.; Ghicov, A.; Tsuchiya, H.; Dick, L. F. P.; Schmuki, P.

Electrochem. Commun. **2006**, 8, 544-548). The atomic percentage for all nitrogen species found in N-doped TiO_2 sample was 1.94 %.

Both TiO_2 and N-doped TiO_2 (TiO_2:N) films were sensitized with CdSe QDs using the CBD method. SEM studies showed that the films were coated with very large particles of ~200 nm in diameter, which were aggregates of smaller CdSe QD. These CdSe aggregates were formed on the surface of the TiO_2 via a "cluster by cluster" growth mechanism (Kale et al. *supra*; Froment, M.; Lincot, D. *Electrochim. Acta* **1995**, 40, (10), 1293-1303). These CdSe sensitized TiO_2 (CdSe-TiO_2) and N-doped TiO_2 (CdSe-TiO_2:N) nanoparticle films were orange in color due to the strong visible absorption of the CdSe QDs. To quantitatively understand the role of N-doping and CdSe sensitization in electronic transitions in TiO_2 nanoparticle films, their UV-visible absorption spectra were measured, as shown in Figure 1(13). All spectra show an apparent absorption peak near 325 nm, which was caused by blanking with a conductive FTO glass substrate. For pristine TiO_2, strong absorption starts around 350 nm, and for TiO_2:N slightly increased absorption of visible light appears in the region of 350-520 nm. The electronic energy level due to substitutional N-doping at O sites (N_o) has been estimated previously, using Density Functional Theory calculations, to be only 0.14 eV above the valence band of TiO_2 (Di Valentin, C.; Pacchioni, G.; Selloni, A.; Livraghi, S.; Giamello, E. *J. Phys. Chem. B* **2005**, 109, (23), 11414-11419). The increased visible absorption for TiO_2:N is thus not likely to be due to electronic transitions from the N_o energy levels to the conduction band of TiO_2. A previous study also indicated that transition from N_o to the conduction band of TiO_2, as mainly originating from a N $2P_\pi$ to Ti d_{xy} transition, is not strong (Tak et al. *supra*). On the other hand, it has been reported that N-doping facilitates the creation of oxygen vacancies (V_o) in TiO_2 lattice (Livraghi, S.; Paganini, M. C.; Giamello, E.; Selloni, A.; Di Valentin, C.; Pacchioni, G. *J. Am. Chem. Soc.* **2006**, 128, (49), 15666-15671; Nambu, A.; Graciani, J.; Rodriguez, J. A.; Wu, Q.; Fujita, E.; Sanz, J. F. *J. Chem. Phys.* **2006**, 125, (9), 094706-094708). In particular, the ammonia annealing process could increase the V_o formation, since H_2 generated from as ammonia breakdown at 530°C can reduce Ti^{4+} to Ti^{3+} (oxygen vacancy) (Irie, H.; Watanabe, Y.; Hashimoto, K. *J. Phys. Chem. B* **2003**, 107, (23), 5483-5486; Wang, J.; Tafen, D. N.; Lewis, J. P.; Hong, Z. L.; Manivannan, A.; Zhi,

M. J.; Li, M.; Wu, N. Q. *J. Am. Chem. Soc.* **2009**, 131, (34), 12290-12297). The formation of V_o creates midgap states about 0.7 - 1.18 eV below the conduction band of TiO_2 (Wang et al. *supra*; Sanjines, R. T., H. Berger, H. Gozzo, F. Margaritondo, G. Levy, F. *J. Appl. Phys.* **1993**, 75, (6), 2945-2951; Thomas, A. G.; Flavell, W. R.; Kumarasinghe, A. R.; Mallick, A. K.; Tsoutsou, D.; Smith, G. C.; Stockbauer, R.; Patel, S.; Grätzel, M.; Hengerer, R. *Phys. Rev. B* **2003**, 67, (3), 035110; Kuznetsov, V. N.; Serpone, N. *J. Phys. Chem. C* **2009**, 113, (34), 15110-15123). The somewhat enhanced visible light absorption of TiO_2:N is therefore attributed to excitation of electrons from the N_o levels to the localized electronic levels of V_o. (See Di Valentin et al. *supra*; Nambu et al. *supra*; Wang et al. *supra*; and Serpone, N. *J. Phys. Chem. B* **2006**, 110, (48), 24287-24293.)

In comparison to TiO_2 and TiO_2:N films, CdSe sensitized TiO_2 films exhibit a significant enhancement in absorption of visible light. Both sensitized films showed similar absorption profile with a dominant peak near 525 nm (Figure 1(13)), which corresponds to the first excitonic absorption of quantum confined CdSe QDs, with an average diameter of ~2.6 nm estimated based on the peak position of the exciton absorption (Yu, W. W.; Qu, L.; Guo, W.; Peng, X. *Chem. Mater.* **2003**, 15, (14), 2854-2860). To the blue of 525 nm, absorption due to transitions to higher electronic states clearly occurs. These excitonic absorptions of CdSe QDs are important for enhancing visible absorption of the CdSe-TiO_2 composites.

Example VI: Photoelectrochemical Studies of Nanoparticles

Photoelectrochemical (PEC) cell studies on four TiO_2 nanoparticle films, TiO_2, TiO_2:N, CdSe-TiO_2 and CdSe-TiO_2:N, have been carried out to understand the effect of N-doping *and* CdSe sensitization on TiO_2 nanoparticle-based photoanode for PEC water splitting. All the PEC studies were conducted in a three-armed cell with a coiled platinum wire as the counter electrode (cathode) and Ag/AgCl double junction reference electrode under nitrogen atmosphere. Photoanodes fabricated from TiO_2 films were made by attaching a copper wire to a bare portion of the FTO conductive glass with a high purity conductive silver paint. Measurements were made on a Solartron 1280B potentiostat using a 1000W Xenon Arc Lamp as the white light source. The electrolyte used was a mixture

of 0.25 M Na_2S and 0.35 M Na_2SO_3 aqueous solution, where Na_2S in solution acts as a hole scavenger and is oxidized into S_2^{2-} to prevent the photocorrosion of CdSe. To ensure efficient hydrogen production at the cathode, Na_2SO_3 was added to reduce disulfides back to sulfides, $S_2^{2-} + SO_3^{2-} \rightarrow S^{2-} + S_2O_3^{2-}$, which has been shown to significantly increase the amount of hydrogen produced (Banerjee, S.; Mohapatra, S. K.; Das, P. P.; Misra, M. *Chem. Mater.* **2008**, 20, (21), 6784-6791; Buehler, N.; Meier, K.; Reber, J. F. *J. Phys. Chem.* **2002**, 88, (15), 3261-3268; Chi, C. F.; Lee, Y. L.; Weng, H. S. *Nanotechnology* **2008**, 19, (12), 125704).

The linear sweep voltammograms recorded from these samples in the dark and with white light illumination of 100 mW/cm^2 are shown in Figure 2(14). The results exhibit several key features. First, all TiO_2 film samples showed a substantial photoresponse, indicating efficient charge separation upon light irradiation. Pristine TiO_2 and TiO_2:N samples showed relatively low steady state photocurrent, ~25 $\mu A/cm^2$. Pristine TiO_2 is expected to be low due to the limited absorption of visible light. However, it is somewhat surprising that the TiO_2:N sample showed more or less the same maximum photocurrent density as the pristine sample. This can be understood in terms of the N doping energy levels in TiO_2. The observed visible light absorption in TiO_2:N is attributed to the electron excitation from N_o levels to V_o levels. Since the V_o levels are located well below the hydrogen reduction potential (H_2O/H_2), they are not able to result in hydrogen generation and thus enhance the photocurrent, which is consistent with our experimental observation.

Second, both CdSe sensitized samples showed a significant enhancement in photocurrent. CdSe-TiO_2 has a steady state photocurrent density of 0.15 mA/cm^2 (Figure 2(14)), which is an order of magnitude enhancement compared to pristine TiO_2 or TiO_2:N. The enhancement is somewhat expected due to strong visible light absorption of CdSe QDs. Significantly, the photocurrent of CdSe-TiO_2:N almost doubles that of CdSe-TiO_2. Since N-doping alone does not noticeably increase the photocurrent and the photocurrent for CdSe-TiO_2:N is much higher than the simple sum of photocurrents for CdSe-TiO_2 and TiO_2:N, a synergistic effect between N-doping *and* CdSe QD sensitization is clearly in operation and responsible for the enhanced photocurrent in CdSe-TiO_2:N compared to CdSe-TiO_2. Due to the importance of this observation, major efforts have been made to

ensure validity of comparison and reproducibility of the results with proper control experiments, including film thickness and light intensity.

Example VII: Model of Physical Chemistry

To better explain the observed trend in photocurrent density of **CdSe-TiO_2:N > CdSe-TiO_2 >> TiO_2 ~ TiO_2:N**, we develop a model based on the relevant electronic states of the different components in these composite nanostructures, as shown in Figure 3(15). The conduction band edge of TiO_2 has been reported to be located at -0.5 eV versus Normal Hydrogen Electrode (NHE), while the conduction band edge of bulk CdSe is close to -0.8 eV versus NHE (Graetzel, M. *Nature* **2001**, 414, 338-344; Wang, C. J.; Shim, M.; Guyot-sionnest, P. *Science* **2001**, 291, 2390-2392). For CdSe QDs, quantum confinement effect makes the energy level of conduction band even more negative (on an NHE scale) with decreasing particle size (Kongkanand, A.; Tvrdy, K.; Takechi, K.; Kuno, M.; Kamat, P. V. *J. Am. Chem. Soc.* **2008**, 130, 4007-4015; Norris, D. J.; Bawendi, M. G. *Phys. Rev. B* **1996**, 53, 16338). This alignment between the conduction band edges of CdSe QDs and TiO_2 nanoparticles should allow for efficient electron transfer from CdSe to TiO_2. Therefore, the photoexcited electrons created in small bandgap CdSe QDs are expected to inject efficiently into TiO_2 nanoparticles and lead to increased photocurrent. More detailed discussion of the model, especially the effect of N-doping, will be given after the IPCE results are disclosed below.

Example VIII: Photoresponse Studies

To further quantify the PEC performance, IPCE measurements have been made to study the photoresponse of the TiO_2 nanoparticle samples with and without CdSe sensitization as a function of incident light wavelength. The IPCE was determined at no bias voltage by the equation:

$$IPCE = (1240 \times I) / (\lambda \times J_{light}) \qquad (6)$$

where I is the photocurrent density, λ the incident light wavelength, and J_{light} is the measured irradiance. Figure 4(16) shows the IPCE results for the different TiO_2 nanoparticle films with and without N doping and/or CdSe QD sensitization. The

unsensitized samples have strong photoresponse in the near UV region but little photoresponse in >400 nm. In contrast, the sensitized samples show substantial photoactivity in the visible light region from 400 to 600 nm in addition to strong photoresponse in the near UV. These results clearly confirm that CdSe sensitization improves the visible light absorption and the photogenerated electrons in CdSe QD can be transferred to TiO_2. While N-doping has little effect on IPCE for the unsensitized sample, it significantly increases the IPCE throughout the entire visible to near UV region for the QD sensitized sample. This again indicates a clear and significant synergistic effect between QD sensitization and N-doping.

In comparison to the undoped sample, TiO_2:N has a higher density of oxygen vacancy states, V_o. It has been proposed that when both V_o and N impurities are present in TiO_2, the electrons from occupied $3d$ states (Ti^{3+}) would transfer to lower energy empty $2p$ states (N^{2-} impurities) (Livraghi et al. *supra*; Nambu et al. *supra*; and Torres, G. R.; Lindgren, T.; Lu, J.; Granqvist, C.-G.; Lindquist, S.-E. *J. Phys. Chem. B* **2004**,108, (19), 5995-6003). This electron transfer mechanism is favorable since it simultaneously lower the formation energy of V_o and stabilize the N impurities (Livraghi et al. *supra*; Nambu et al. *supra*; and Torres et al. *supra*). We suggest that this electron transfer process results in partially occupied V_o levels located at ~0.4 eV above the CdSe valence band edge (as shown in Figure 3(15)) that can facilitate hole transfer from CdSe to TiO_2 following photoexcitation of the CdSe QDs. This interfacial hole transfer could improve the PEC photocurrent of CdSe-TiO_2:N nanoparticle films in two ways. First, it can lead to reduction in electron-hole recombination in CdSe QDs. Second, the holes transferred to the V_o levels in TiO_2 can either oxidize the sacrificial reagent on site or be further transported through the TiO_2 network to other oxidation sites, the latter being especially important for thick nanocrystalline films. Both processes are expected to lead to enhanced conversion efficiency of light to photocurrent. This explanation is consistent with all the UV-vis and IPCE results. This model is also modified from the previous model we proposed to explain enhanced photoresponse in CdSe-TiO_2:N films for photovoltaic cells where N-doping was thought to directly facilitate hole transport (Lopez-Luke et al. *supra*). The present novel results strongly suggest that the enhancement in photoresponse for the

QD-sensitized *and* N-doped TiO_2 is due to improved hole transfer/transport enhanced by oxygen vacancy states mediated by N-doping. Detailed kinetic studies on the interfacial carrier transfer between CdSe QD and TiO_2 need to be carried out in the future.

Example IX: Photoelectrochemical Studies of Nanowires

To confirm this enhanced hole transfer/transport model first developed for zero-dimensional (0D) TiO_2 nanoparticle films and extend it to one-dimensional (1D) nanostructures, we have also conducted photoelectrochemical (PEC) studies on different TiO_2 nanowire samples (TiO_2, TiO_2:N, CdSe-TiO_2 and CdSe-TiO_2:N). High density and vertically aligned TiO_2 nanowire arrays were grown on FTO glass using a hydrothermal method. Electron microscopy studies showed that the as-prepared nanowires are single crystal rutile structures and are uniform with diameters in the range from ~100 nm to 150 nm. The typical nanowire lengths are 2 - 3 μm, which depends on the growth time. These TiO_2 nanowire arrays were N-doped in ammonia and sensitized with CdSe QDs using the CBD method, as for TiO_2 nanoparticles. The linear sweep voltammograms recorded from these samples in dark and with light illumination of 100 mW/cm^2 are illustrated in Figure 5(17). TiO_2 nanowires exhibit a pronounced photocurrent density of 0.5 mA/cm^2 at -0.2 V vs. Ag/AgCl. The maximum photocurrent density of TiO_2:N nanowires is similar to that of the pristine sample, as expected. Significantly, both TiO_2 and TiO_2:N nanowire samples showed a great enhancement in photocurrent after CdSe sensitization. In particular, the electrode with the greatest photocurrent density of 2.75 mA/cm^2 is the CdSe-TiO_2:N nanowires, showing almost two times enhancement compare to CdSe-TiO_2 nanowires. These experimental observations are fully consistent with those obtained for TiO_2 nanoparticle samples in terms of the synergistic effect between QD sensitization and N-doping and indicate that the proposed enhanced hole transfer/transport model is valid for both anatase and rutile TiO_2 nanostructures in 0D or 1D. In addition, it is noted that the TiO_2 nanowire-based photoanodes have almost an order of magnitude higher photocurrent density than that of the TiO_2 nanoparticle-based photoanodes. This enhancement can be attributed to improved vectorial charge transport in 1D structures and/or the increased thickness of nanowire film.

Those skilled in the art will appreciate that various adaptations and modifications of the just-described embodiments can be configured without departing from the scope and spirit of the invention. Other suitable techniques and methods known in the art can be applied in numerous specific modalities by one skilled in the art and in light of the description of the present invention described herein. Therefore, it is to be understood that the invention can be practiced other than as specifically described herein. The above description is intended to be illustrative, and not restrictive. Many other embodiments will be apparent to those of skill in the art upon reviewing the above description. The scope of the invention should, therefore, be determined with reference to the appended claims, along with the full scope of equivalents to which such claims are entitled.

We claim:

1. A thin film structure comprising a conducting substrate, a thin layer comprising nanocrystalline metal oxide doped with nitrogen thereon, and further comprising a semiconductor quantum dot and a linker thereon said thin layer of crystalline metal oxide.

2. The thin film structure of claim 1 wherein the conducting substrate is selected from the group consisting of indium tin oxide and fluorine tin oxide.

3. The thin film structure of claim 1 wherein the nanocrystalline metal oxide is selected from the group consisting of titanium dioxide, tungsten oxide, and zinc oxide.

4. The thin film structure of claim 1 wherein the semiconductor quantum dot is selected from the group consisting of cadmium selenium and cadmium telluride.

5. The thin film structure of claim 1 wherein the linker is selected from the group consisting of thioglycolic acid (TGA), mercaptopropanoic acid (MPA), and cysteine.

6. The thin film structure of claim 1 wherein the linker links the semiconductor quantum dot with the conducting substrate.

7. A photovoltaic cell comprising the thin film structure of claim 1.

8. A hydrogen synthesis system comprising the photovoltaic cell of claim7.

9. The hydrogen synthesis system of claim 8 further comprising hydrogen storage means wherein the hydrogen is stored therein.

10. The hydrogen synthesis system of claim 9 wherein the hydrogen is stored as a phase selected from the group consisting of a gas, a liquid, and as a liquid or gas in a composition, the composition comprising a plurality of cavities.

11. The photovoltaic cell of claim 7 having a power conversion efficiency of between 1 10^{-3} and 5 η%.

12. The photovoltaic cell of claim 11 having a power conversion efficiency of between 5 10^{-3} and 1 η%.

13. The photovoltaic cell of claim 7 having an incident photon to current conversion efficiency (IPCE) of between 1% and 99%.

14. The photovoltaic cell of claim 13 having an IPCE of between 13% and 95%.

15. The photovoltaic cell of claim 13 having an IPCE of between 25% and 90%.

16. The photovoltaic cell of claim 13 having an IPCE of between 50% and 85%.

17. A method for generating an electric current, the method comprising the steps of (i) providing a conducting substrate; (ii) doping a nanocrystalline metal oxide with nitrogen; (iii) depositing said nanocrystalline metal oxide doped with nitrogen upon said conducting substrate; (iv) providing a semiconductor quantum dot; (v) linking said semiconductor quantum dot to said conducting substrate using a linker; (vi) irradiating the surface of said conducting substrate with photons from a photon source thereby creating or inducing an electric current through the conducting substrate; the method thereby generating an electric current.

18. The method of claim 17 wherein the conducting substrate is selected from the group consisting of indium tin oxide and fluorine tin oxide.

19. The method of claim 17 wherein the crystalline metal oxide is selected from the group consisting of titanium dioxide, tungsten oxide, and zinc oxide.

20. The method of claim 17 wherein the semiconductor quantum dot is selected from the group consisting of cadmium selenium and cadmium telluride.

21. The method of claim 17 wherein the linker is selected from the group consisting of thioglycolic acid (TGA), mercaptopropanoic acid (MPA), and cysteine.

22. The method of claim 17 wherein the photons from the photon source have power intensity of between 1 and 10000 mW/cm^2.

23. The method of claim 17 wherein the photons from the photon source have power intensity of between 10 and 1000 mW/cm^2.

24. The method of claim 17 wherein the photons from the photon source have power intensity of between 25 and 250 mW/cm^2.

25. The method of claim 24 wherein the photons from the photon source have power intensity of 100 mW/cm^2.

26. The method of claim 24 wherein the photons from the photon source have power intensity of 27 mW/cm^2.

27. A method for generating hydrogen, the method comprising the steps of (i) providing a conducting substrate; (ii) doping a nanocrystalline metal oxide with nitrogen; (iii) depositing said nanocrystalline metal oxide doped with nitrogen upon said conducting

substrate; (iv) providing a semiconductor quantum dot; (v) linking said semiconductor quantum dot to said conducting substrate using a linker; (vi) providing a hydrogen source in contact with the opposing surface of said conducting substrate; (vii) irradiating the surface of said conducting substrate with photons from a photon source thereby creating or inducing an electric current through the conducting substrate; (viii) allowing the electric current to electrolyze the hydrogen source, thereby producing hydrogen; the method thereby generating hydrogen.

28. The method of claim 27 wherein the conducting substrate is selected from the group consisting of indium tin oxide and fluorine tin oxide.

29. The method of claim 27 wherein the crystalline metal oxide is selected from the group consisting of titanium dioxide, tungsten oxide, and zinc oxide.

30. The method of claim 27 wherein the semiconductor quantum dot is selected from the group consisting of cadmium selenium and cadmium telluride.

31. The method of claim 27 wherein the linker is selected from the group consisting of thioglycolic acid (TGA), mercaptopropanoic acid (MPA), and cysteine.

32. The method of claim 27 wherein the hydrogen source is selected from the group consisting of methanol, ethanol, water, formic acid, and an amine compound.

33. The method of claim 27 wherein the photons from the photon source have power intensity of between 1 and 10000 mW/cm^2.

34. The method of claim 27 wherein the photons from the photon source have power intensity of between 10 and 1000 mW/cm^2.

35. The method of claim 27 wherein the photons from the photon source have power intensity of between 25 and 250 mW/cm^2.

36. The method of claim 35 wherein the photons from the photon source have power intensity of 100 mW/cm^2.

37. The method of claim 35 wherein the photons from the photon source have power intensity of 27 mW/cm^2.

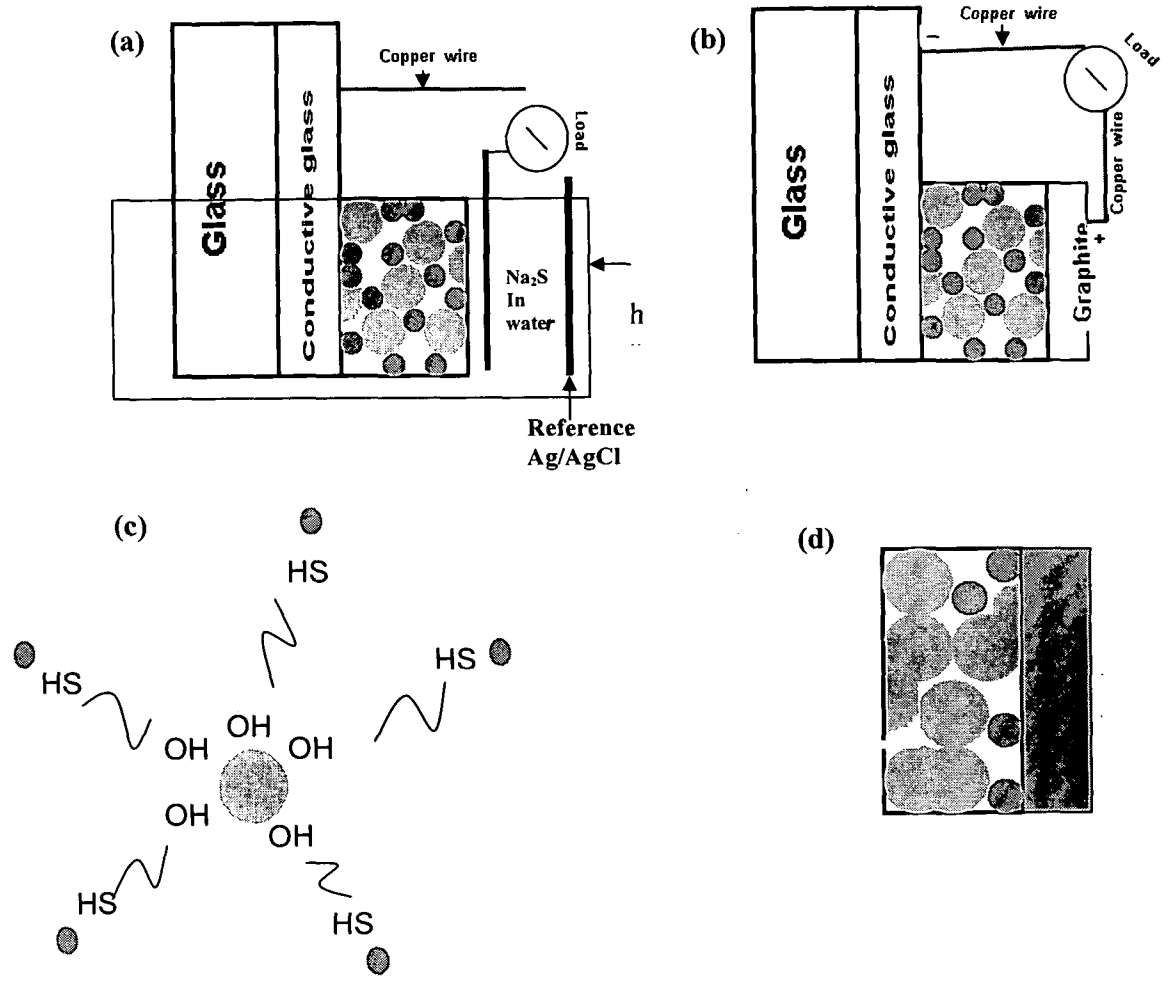
(a)
Copper wire
Load
Glass
Conductive glass
Na_2S
In
water
h
Reference
Ag/AgCl
(b)
Copper wire
Load
Glass
Conductive glass
Copper wire
Graphite
(c)
HS
HS
HS
OH
OH
OH
OH
OH
HS
HS
(d)

Figure 1

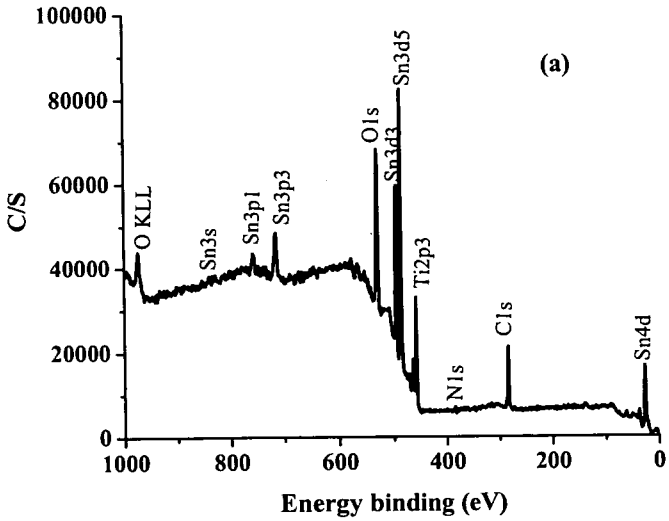
100000
80000
60000
40000
20000
0
C/S
(a)
O KLL
Sn3s
Sn3p1
Sn3p3
O1s
Sn3d3
Sn3d5
Ti2p3
N1s
C1s
Sn4d
1000
800
600
400
200
0
Energy binding (eV)

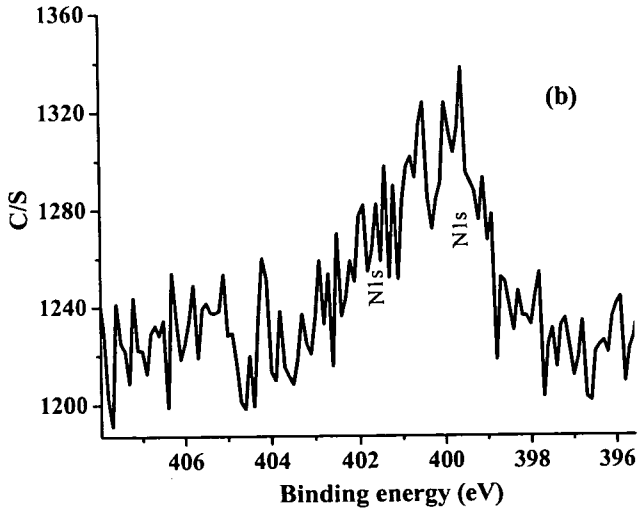
1360
1320
1280
1240
1200
C/S
(b)
N1s
N1s
406
404
402
400
398
396
Binding energy (eV)

Figure 2

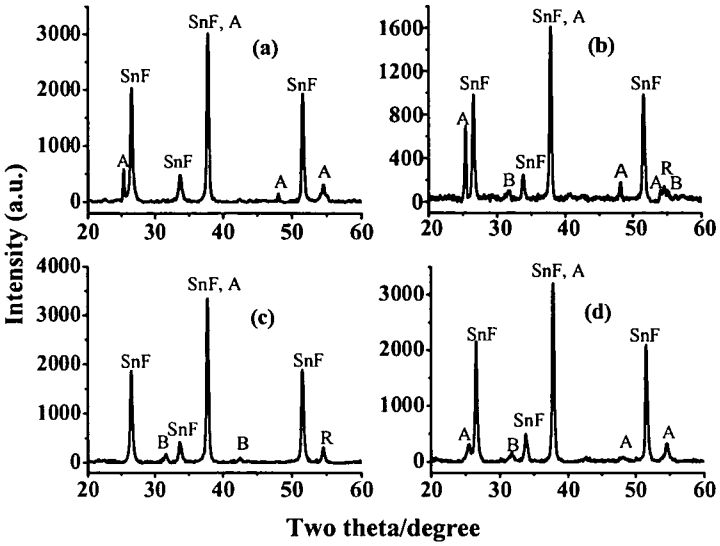

Figure 3

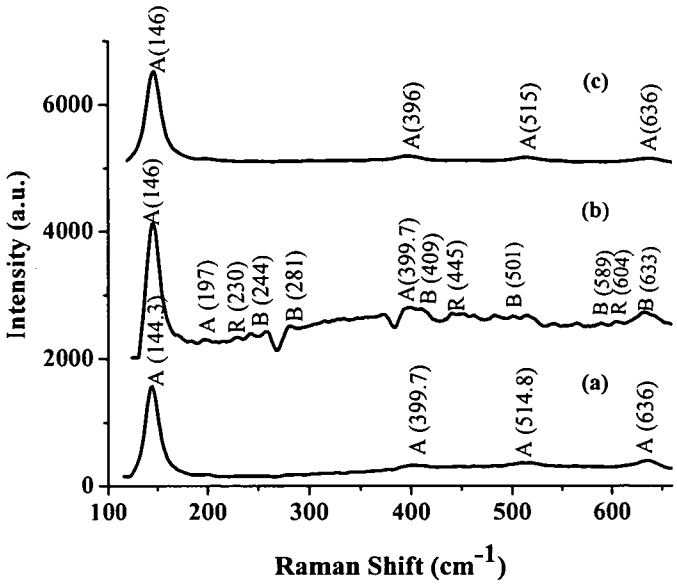

Figure 4

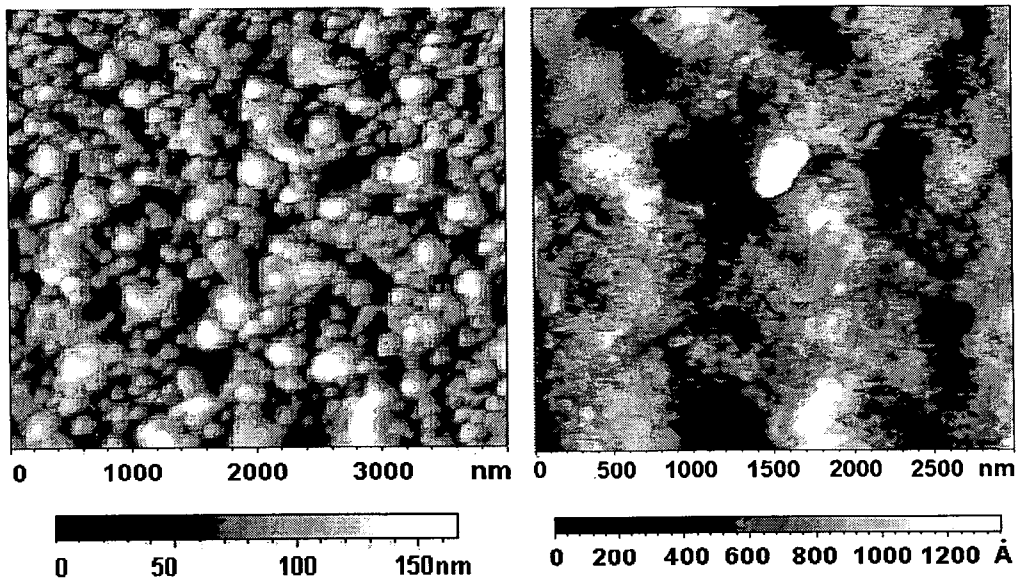

Figure 5

Figure 6

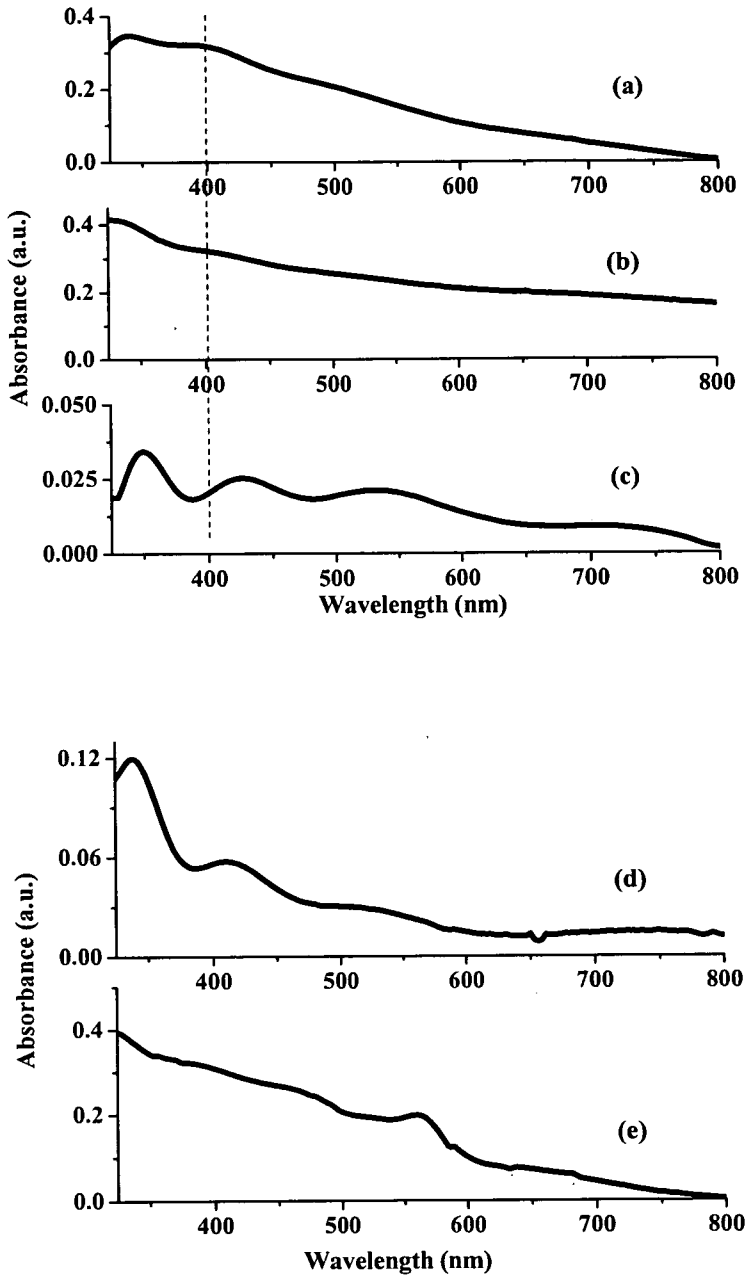
0.4
0.2
0.0
(a)
400
500
600
700
800
Absorbance (a.u.)
0.4
0.2
0.0
(b)
400
500
600
700
800
0.050
0.025
0.000
(c)
400
500
600
700
800
Wavelength (nm)
0.12
0.06
0.00
(d)
400
500
600
700
800
Absorbance (a.u.)
0.4
0.2
0.0
(e)
400
500
600
700
800
Wavelength (nm)

Figure 7

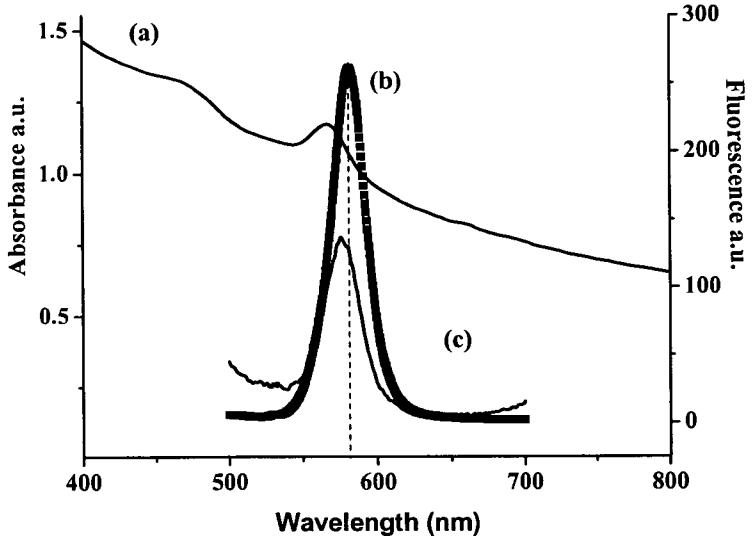

Figure 8

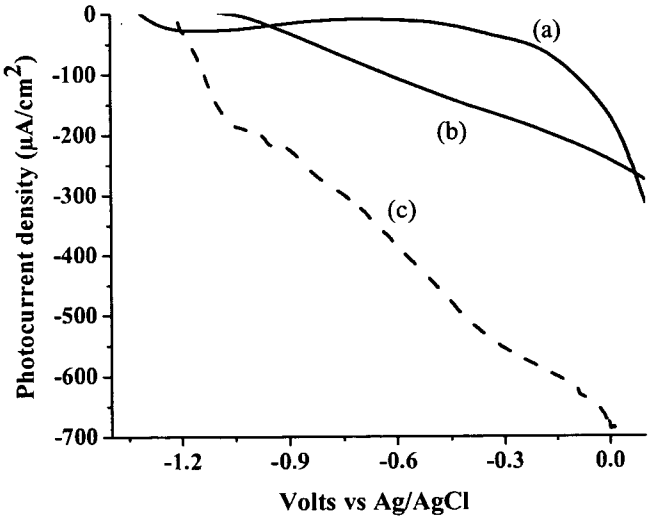

Figure 9

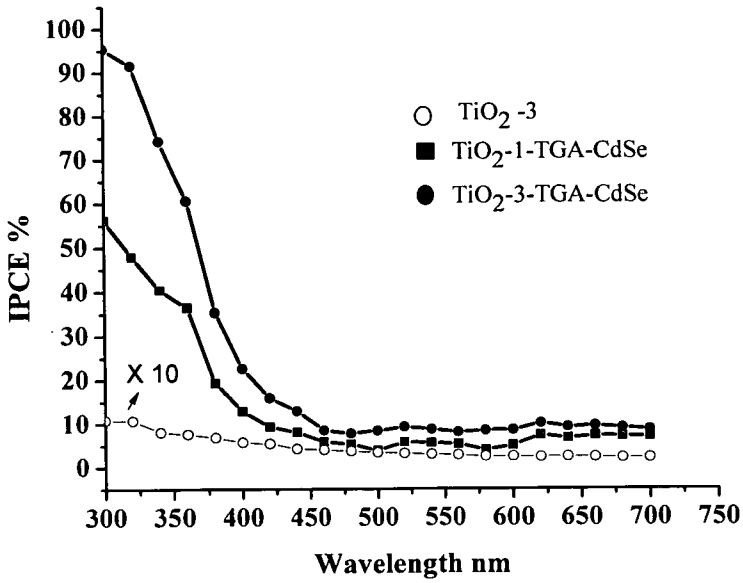

Figure 10

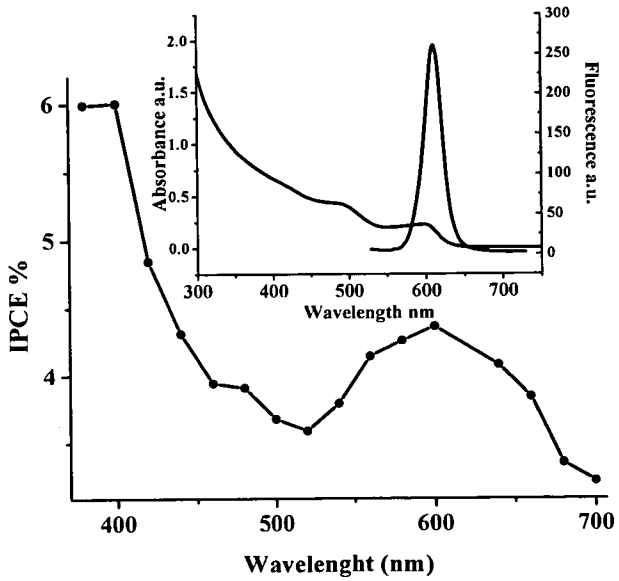

Figure 11

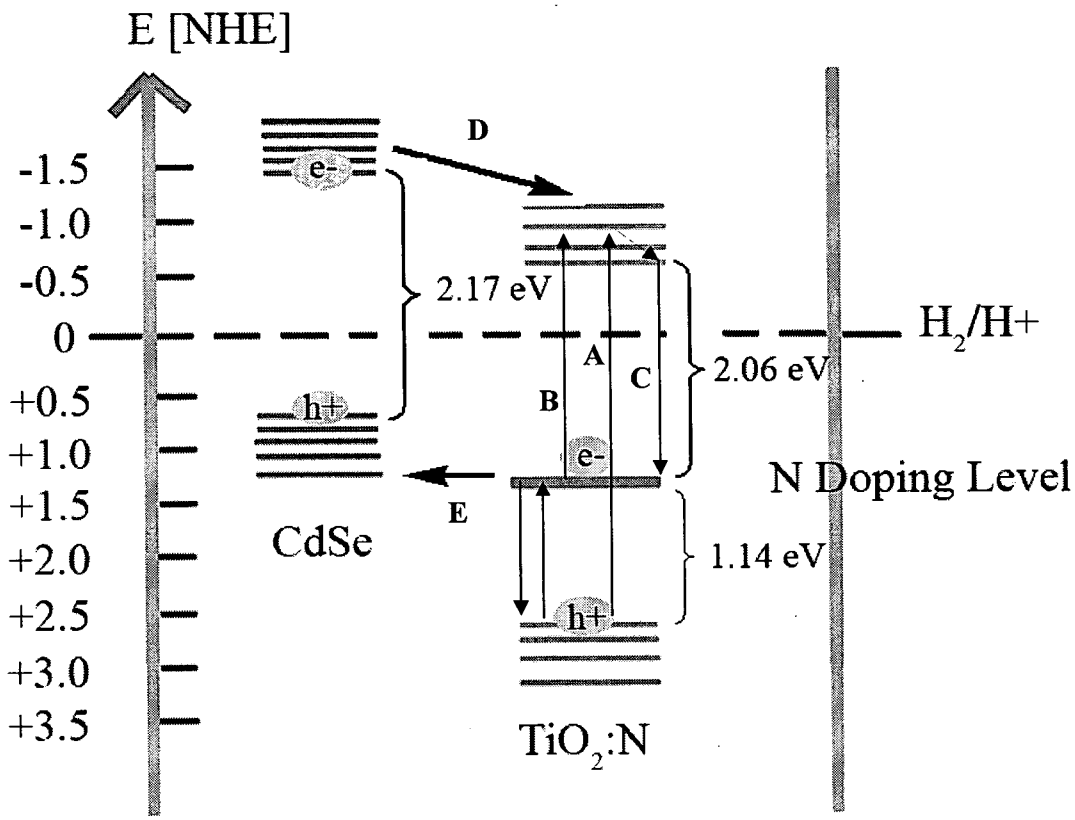
E [NHE]
-1.5
-1.0
-0.5
0
+0.5
+1.0
+1.5
+2.0
+2.5
+3.0
+3.5
e-
h+
D
2.17 eV
A
B
C
2.06 eV
H2/H+
e-
E
CdSe
N Doping Level
1.14 eV
h+
TiO2:N

Figure 12

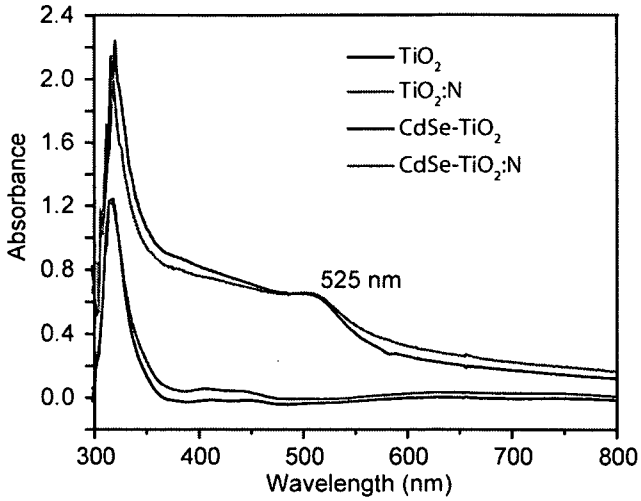

Figure 13

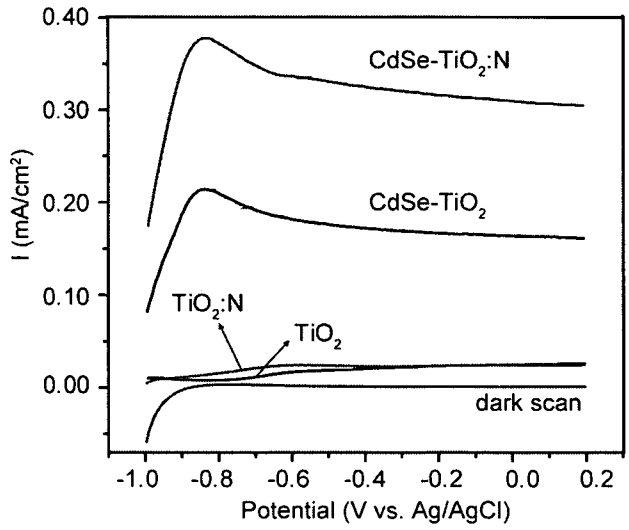

Figure 14

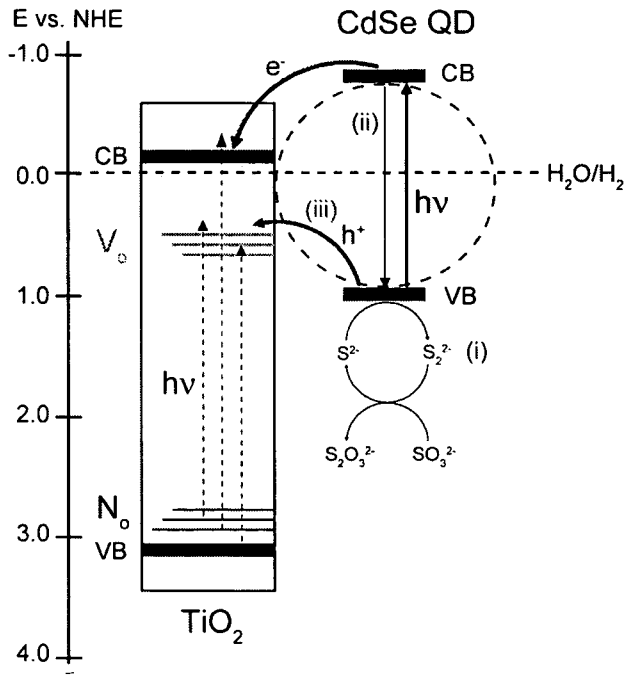

Figure 15

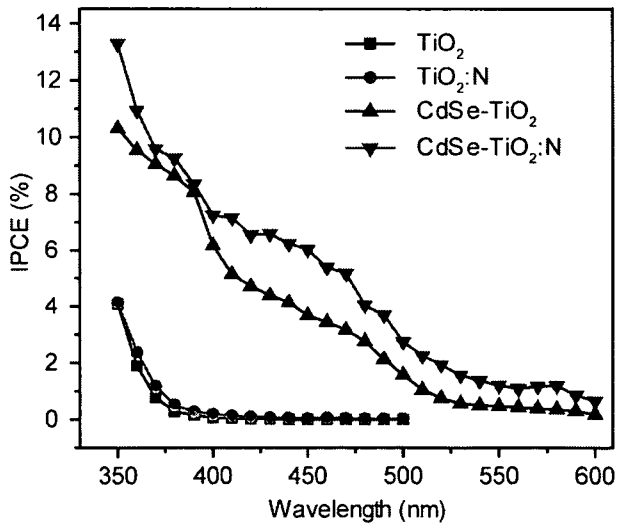

Figure 16

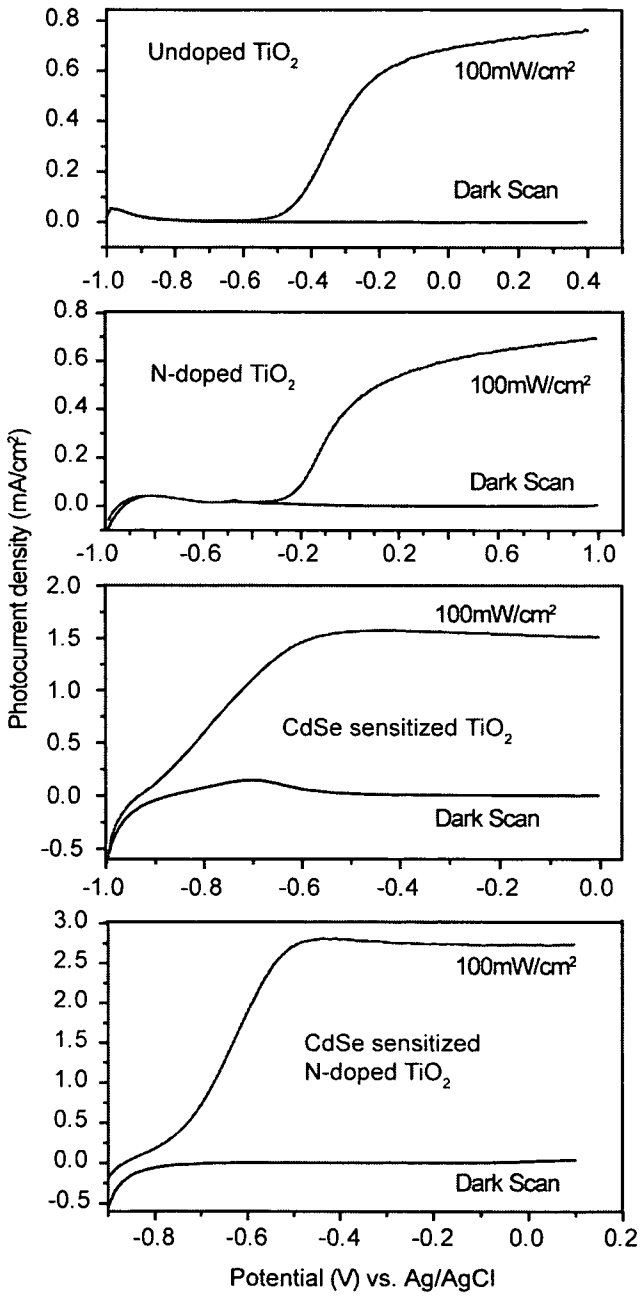
Undoped TiO2
100mW/cm2
Dark Scan
N-doped TiO2
100mW/cm2
Dark Scan
100mW/cm2
CdSe sensitized TiO2
Dark Scan
100mW/cm2
CdSe sensitized
N-doped TiO2
Dark Scan
Photocurrent density (mA/cm2)
Potential (V) vs. Ag/AgCl

Figure 17

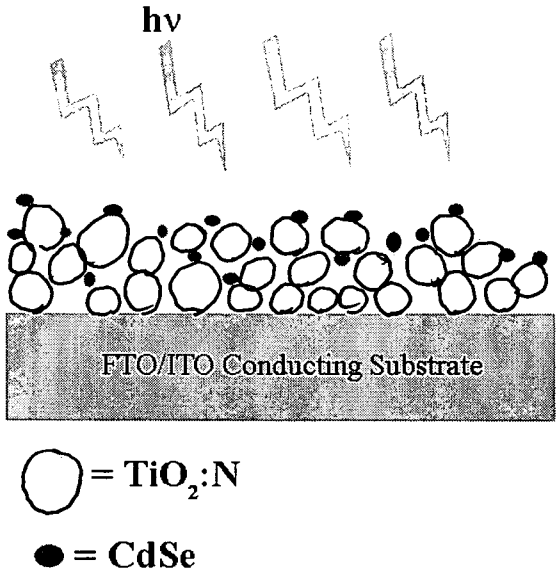

Figure 18